NASA Technical Memorandum 100708

Data Report for the Siple Coast Project

R. A. Bindschadler, S. N. Stephenson,
E. P. Roberts, D. R. MacAyeal,
and D. R. Lindstrom

OCTOBER 1988

NASA

NASA Technical Memorandum 100708

Data Report for the Siple Coast Project

R. A. Bindschadler
Goddard Space Flight Center
Greenbelt, Maryland

S. N. Stephenson
Science Applications Research
Lanham, Maryland

E. P. Roberts
Department of Geology,
University of Maryland
College Park, Maryland

D. R. MacAyeal and D. R. Lindstrom
Department of Geophysical Sciences
University of Chicago
Chicago, Illinois

National Aeronautics and
Space Administration

Scientific and Technical
Information Office

1988

CONTENTS

LIST OF FIGURES

LIST OF TABLES

INTRODUCTION

This report contains a compilation of the data collected by a combined NASA/University of Chicago field program on Siple Coast, Antarctica from October 1983 to January 1987 and a description of the methods used to obtain the data. In its first three field seasons, beginning in October 1983, the project has concentrated on studying Ice Streams B and C (see Figure 1). A number of publications have resulted from the analysis of these data and they are referenced in Appendix 4. This report will assist in the continuing analysis of these data and adds them to the growing data base that exists for the region.

The NASA/University of Chicago program is part of a larger project which also involves the Byrd Polar Research Center at Ohio State University and the Geophysical and Polar Research Center at the University of Wisconsin. The major goals of this larger project are:

1) To measure the mass balance and configuration of the major ice streams in the Ross Sea drainage basin of the West Antarctic ice sheet;

2) To determine the forces that control the flow of these ice streams;

3) To investigate long-term trends in the drainage basin.

To meet these goals, the NASA/University of Chicago group designed a data acquisition operation with the following specific objectives:

1) Establish a network of stations to measure the surface velocity and strain rate profiles across the widths of Ice Streams B and C at locations near their grounding lines to determine net ice stream discharge rates.

2) Establish stake schemes to measure longitudinal velocity and strain rate profiles to determine the spatial gradients of both ice transport and the forces which restrain the ice stream motion.

3) Establish a network of stations which surround Crary Ice Rise (Figure 1), to measure velocities and strain rates, and thus determine its influence on the flow of Ice Stream B, and the state of mass balance of the ice rise.

4) Establish a network of stations which surround a feature named Ice Rise "a", a feature seen on early airborne photography in the region, to determine its position and characteristics. (We state here that Ice Rise "a" is not a true ice rise at all, as its velocity is the same as the surrounding ice, which is itself, lightly grounded.)

5) Establish a network of stations to measure the ice velocity and strain rate fields in the lower, lightly grounded regions of Ice Stream B referred to as the "ice plain".

6) Map the precise location of the grounding lines of Ice Streams B and C.

7) Perform regional studies of small-scale ice rumples to characterize their effect on the large-scale flow.

8) Establish stake schemes and carry out resection surveys to measure the velocity field in the severely crevassed margins of both ice streams and ice rises, to determine the local stresses in this region.

9) Develop a new method for rapid acquisition of strain rate data using multi-leg rosettes.

Although the data presented within this report are mainly the result of the collaborative effort of the University of Chicago

and NASA, the wider collaboration with Ohio State University and the University of Wisconsin is also evident, particularly in the map figures. We have used the results published in Shabtaie and Bentley (1986) as the basis for the boundaries of the ice streams and their grounding lines and the radar definition of ice rises and rumples. We are also grateful for vigorous continuing discussions between the authors and the other collaborating institutes; in particular, with S. Shabtaie, C. R. Bentley and I. M. Whillans.

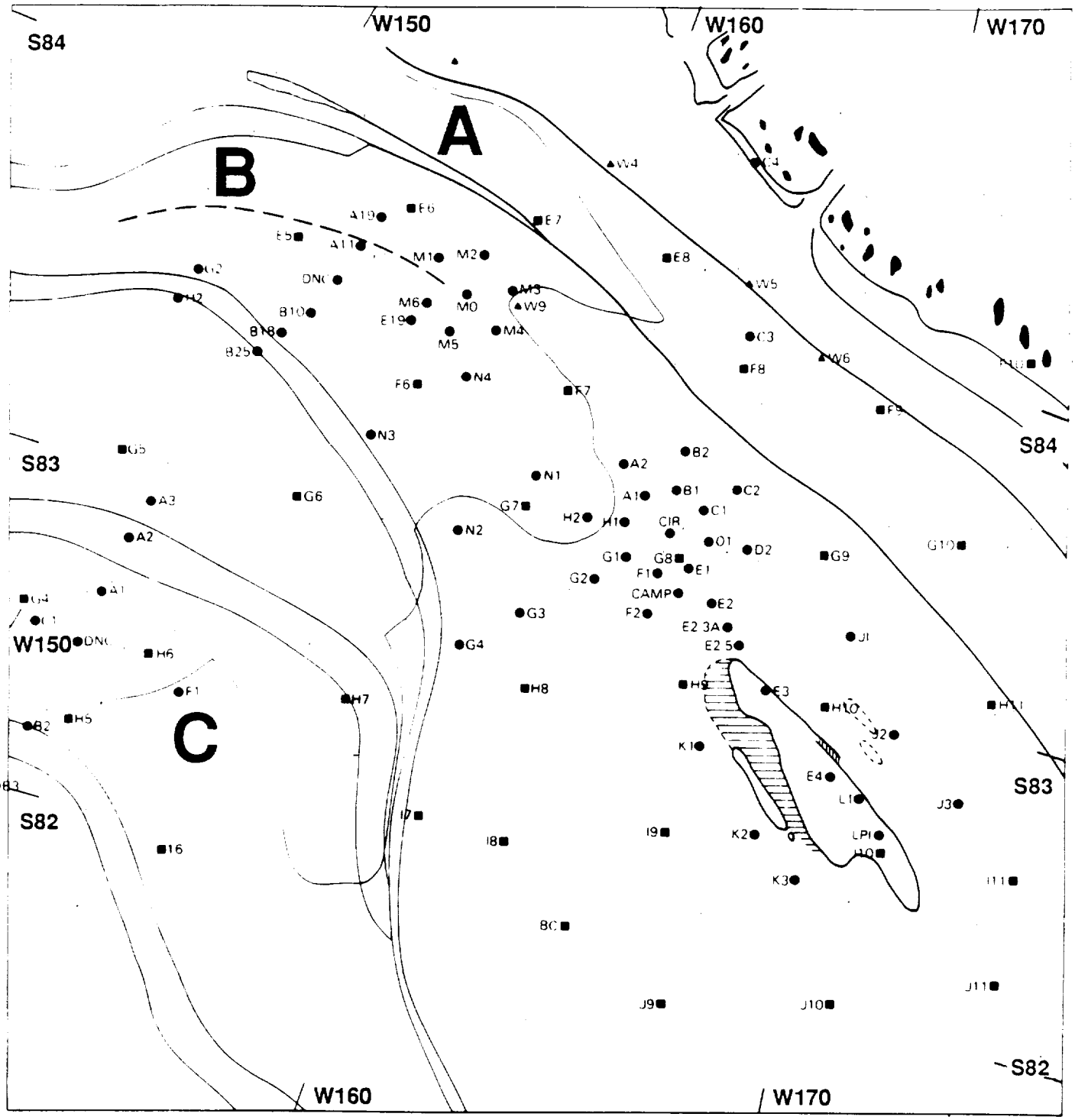

Figure 1: Regional map showing station positions.

SECTION 1: ICE VELOCITY

During this program, 26 ice velocities were measured by accurately determining the position of stakes using a Doppler satellite tracking system at several times and then calculating the distance moved during the time intervals. To obtain the distance between two geographic positions, Clarke's formulae were used, (see Jackson 1980), with a value for the semi-major axis of 6378.16 km and a flattening of 1/298.25.

A Magnavox MX1502 geoceiver was used for precise position determination. Each successful tracking of a satellite pass provides an independent fix of the receiver position. Successive fixes are averaged together by the receiver so that after about 30 passes, the position reaches a steady value within a sphere of about a 1.6-meter radius. However, this value of the standard deviation cannot be considered the error in absolute position because there is also an error in the broadcast satellite ephemeris which can cause an additional error of up to 20 meters (Whillans, personal communication). This imprecision can be improved with post-processing by using either precise ephemerides or translocation techniques. To obtain 30 passes at 84 degrees south, the average latitude of the field program, the geoceiver must operate for about 24 hours. For operational reasons, a geoceiver was rarely allowed to track more than 40 passes. More often, only about 10 passes were used to obtain a position.

We have adopted the error analysis of Thomas et al (1984) in which for less than 30 passes, they take the root-mean-square radial error as $17.48/\sqrt{n}$ meters, where n is the number of passes used to obtain a point position. This is twice the error found during the geoceiver test program and about 1.5 times larger than the error calculated by the Magnavox MX1502, but we feel this larger error should be used, given the lack of any other control. This error indicates that for ice moving at a velocity greater than 150 m/a, and a measurement interval of at least 1 year, as

few as 10 passes will give the velocity to within 5 percent; 30 passes will reduce the error to less than 3 percent. For ice moving 100 m/a, 30 point positions are needed to give 5 percent accuracy, while for ice moving at 30 m/a, translocation methods are needed to obtain better than 10 percent accuracy.

Table 1 summarizes the velocities measured by geoceivers. It includes the latitude and longitude of each station, the date at which the original position was observed, the number of passes for the two point position determinations, and the velocity magnitude and direction along with an estimate of their errors. Our computed velocities and those of the Ross Ice Shelf Geophysical and Glaciological Survey (RIGGS) program are plotted in Figure 2.

Table 2 gives the velocity across a 54-km width of Ice Stream B, including station DNB. The width of the glacier at this point is 84 $\pm$ 3 km taken from the map in Shabtaie and Bentley (1987). The velocities were determined by transecting a line of stakes twice to determine their relative positions and motion, and then adding the velocity determined by Doppler satellite positioning at station DNB. The observations were made over two 1-year time intervals; stakes A11 to B10 were surveyed in 1983 and 1984, and stakes B11 to B19 were surveyed in 1984 and 1985 so all the observations were reduced to two epochs. The rotation of the stake line (about 6 minutes in 2 years) was included in these calculations. The velocity at stake B18 was also determined by Doppler satellite positioning. The misclosure between the two methods is 5 meters in magnitude and 5 degrees in azimuth, which corresponds to a 26-meter error for both positions each time they were measured. Figure 3 plots the transverse velocity profile.

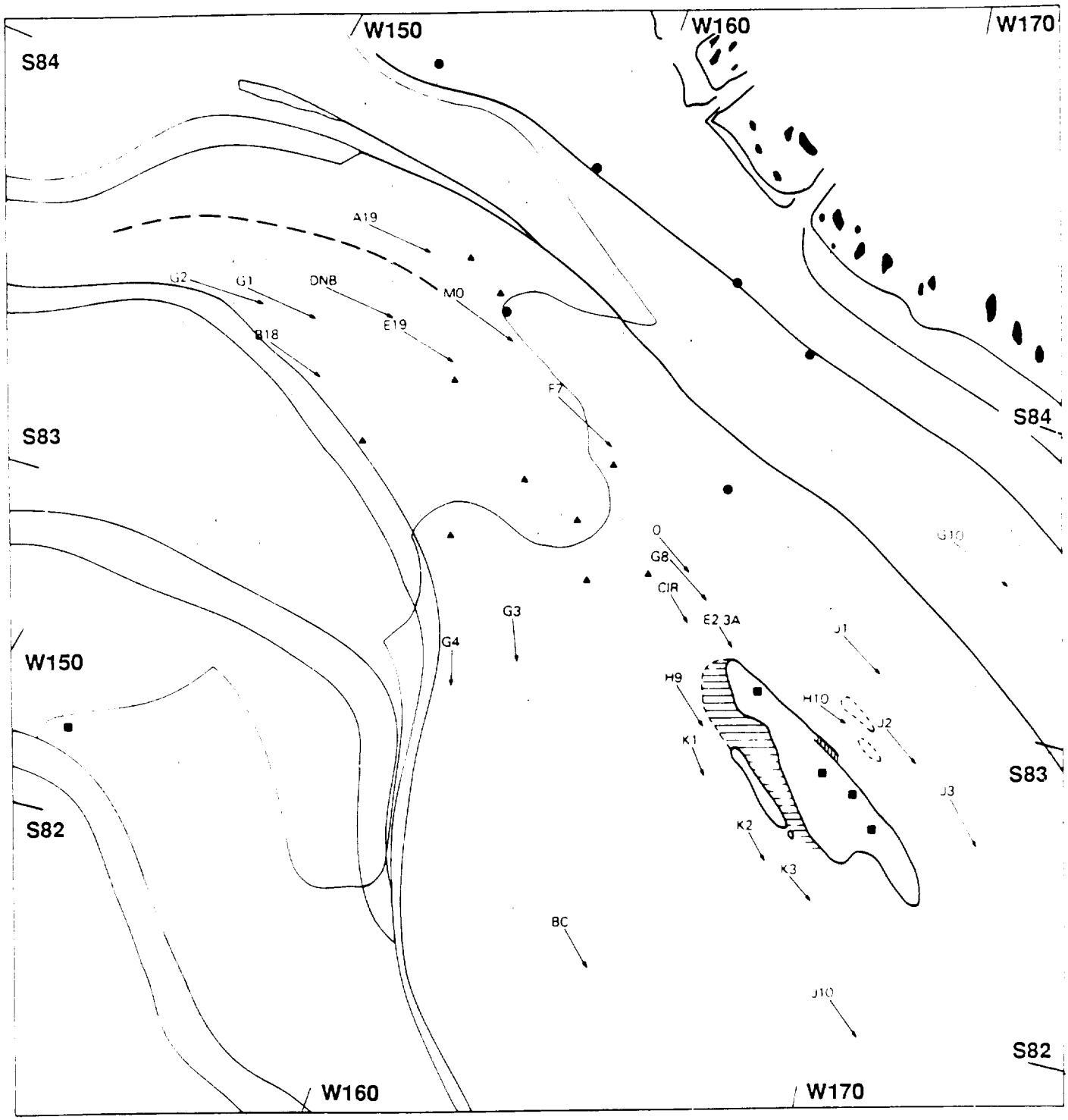

Figure 2: Regional map showing station velocities.

TABLE 1 VELOCITY MEASUREMENTS

Site	Latitude	Longitude	No. of Passes	Velocity Magnitude	Velocity Azimuth*	Date
	deg/min/sec	deg/min/sec	YR1 YR2	(m/a)	(deg)	D/M/Y
Crary						
E2.3A	83 33 09.1	168 12 43	17 9	172 ± 7	319 ± 2	30.1 11 84
E3	83 22 44.0	169 34 33	6 30	21 8	144 21	19.7 11 84
E4	83 9 20.2	171 36 38	15 7	7 8	23 49	19.9 11 84
K1	83 10 24.3	168 9 9	5 8	225 10	326 3	20.1 11 84
K2	82 56 34.9	169 58 00	7 8	224 9	323 2	20.2 11 84
K3	82 49 26.6	171 09 52	13 4	239 10	313 2	25 11 84
J1	83 35 26.7	171 35 34	6 11	387 9	310 1	20.4 11 84
J2	83 19 3.8	173 04 26	3 15	333 11	314 2	20 11 84
J3	83 7 22.4	174 55 29	18 16	385 6	329 1	27.9 11 84
C4	84 57 52.1	165 38 44	1 14	75 18	25 13	23.0 11 84
G3	83 25 42.3	162 43 12	5 9	312 10	338 2	21 11 84
G4	83 16 40.0	161 26 55	2 20	264 14	342 3	23.2 11 84
L1	83 06 11.8	172 25 21	25 40	15 5	333 17	26.2 11 84
LP1	83 00 04.3	172 59 57	9 20	16 7	126 24	28.1 11 84
O	83 47 14.0	166 01 28	8 10	369 8	304 1	30.9 11 84
CAMP	83 37 14.4	166 44 31	17 28	245 5	318 1	17.0 11 84
Downstream B						
MO	84 17 45.9	158 10 58	12 23	471 6	285 1	4 12 84
DNB	84 10 27.6	154 18 43	45 23	517 5	269.5 0.5	19.4 12 84
E19	84 9 3.1	156 51 07	5 38	465 8	279 1	7.2 12 84
G1	84 3 57.6	152 08 59	5 4	534 12	269 1	12.3 12 84
G2	84 0 28.2	150 32 03	17 11	551 7	259.9 0.7	15.9 12 84
A19	84 24 26.5	154 42 21	15 20	487 6	270.6 0.7	11.2 12 84
B18	83 57 00.1	153 33 32	12 23	426 6	279.1 0.8	9.0 12 84
B25	83 52 01.8	153 10 38	4 23	13 9	268 38	9.3 12 84
H2	83 53 49.0	150 25 25	19 38	30 5	203 10	17.3 12 84
Downstream C						
H5	82 35 25	153 14 54	27	6 .5	321 7	12 12 84

*All azimuths are measured clockwise from true North

TABLE 2 VELOCITIES ACROSS ICE STREAM B MEASURED BY TRANSECT

STATN	LAT	LONG	X	Y	VELOCITY Magnitude	Azim.	Bearing*
	deg/min/sec	deg/min/sec	km	km	m/a	deg	deg X
B19	83 55 58.1	153 24 01	301.68	602.45	386.1± 0.6	274.3	210.9
B18	83 56 56.9	153 30 11	299.79	601.36	431.2 0.5	274.3	210.8
B17	83 57 38.0	153 34 07	298.54	600.57	445.9 0.5	274.3	210.7
B16	83 58 18.6	153 38 04	297.29	599.79	455.4 0.4	274.1	210.5
B15	83 58 59.9	153 42 06	296.02	598.99	462.3 0.4	274.0	210.3
B14	83 59 42.8	153 46 20	294.69	598.17	467.6 0.4	273.9	210.1
B13	84 00 21.9	153 50 13	293.49	597.41	471.8 0.4	273.6	209.8
B12	84 01 03.9	153 54 24	292.19	596.61	475.9 0.3	273.5	209.6
B11	84 01 45.6	153 58 33	290.90	595.80	480.0 0.3	273.3	209.3
B10	84 02 42.2	154 04 15	289.15	594.71	485.6 0.3	273.1	210.0
B9	84 03 29.5	154 05 25	288.31	593.49	490.4 0.2	272.7	208.6
B8	84 04 14.9	154 06 32	287.50	592.32	494.7 0.2	272.5	208.3
B7	84 04 59.8	154 07 40	286.70	591.17	498.8 0.2	272.0	207.9
B6	84 05 46.0	154 08 49	285.88	589.98	502.2 0.2	271.6	207.5
B5	84 06 32.9	154 10 00	285.05	588.78	506.2 0.2	271.2	207.0
B4	84 07 19.8	154 11 11	284.21	587.57	509.8 0.1	270.7	206.5
B3	84 08 06.2	154 12 22	283.39	586.38	512.9 0.1	270.3	206.1
B2	84 08 52.5	154 13 33	282.56	585.19	515.0 0.1	270.0	205.8
B1	84 09 41.2	154 14 48	281.70	583.93	516.2 0.1	269.8	205.5
DNB			280.87	582.74	517.0 0.1	269.0	
A1	84 11 10.3	154 17 06	280.11	581.64	517.7 0.1	269.6	205.3
A2	84 11 56.7	154 18 19	279.28	580.45	518.0 0.1	269.4	205.1
A3	84 12 41.7	154 19 28	278.49	579.29	517.8 0.1	269.0	204.7
A4	84 13 25.6	154 20 37	277.71	578.16	518.1 0.2	268.7	204.3
A5	84 14 12.3	154 21 50	276.88	576.96	517.4 0.2	268.3	204.0
A6	84 14 45.4	154 22 43	276.29	576.10	517.1 0.2	268.1	203.7
A7	84 15 31.9	154 23 56	275.46	574.91	516.2 0.2	267.9	203.5
A8	84 16 02.2	154 24 44	274.92	574.18	515.7 0.2	267.8	203.4
A9	84 16 49.0	154 26 04	274.08	572.93	516.0 0.3	267.7	203.3
A10	84 17 19.3	154 26 57	273.53	572.15	516.8 0.3	267.6	203.2
A11	84 18 05.1	154 28 15	272.70	570.98	517.7 0.3	267.7	203.3

*Bearing is given as angle clockwise from positive X-axis. At station A1, positive X-axis is oriented 64.3 degrees clockwise from true North.

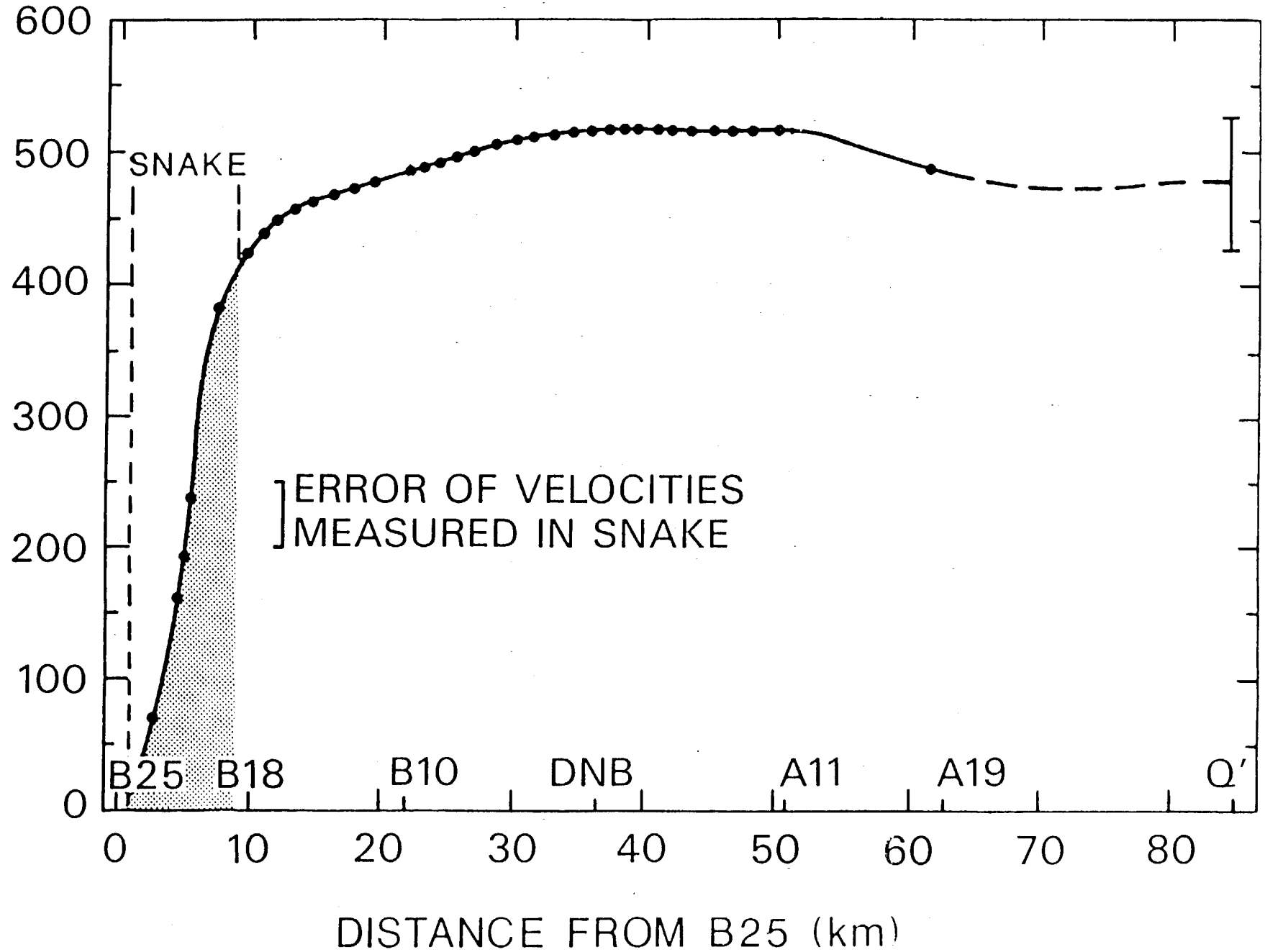

Figure 3: Velocities across Ice Stream B.

SECTION 2: STRAIN RATE AND ROTATION

The rate of deformation at the surface of an ice sheet with respect to mutually perpendicular axes (x, y and z) can be expressed by the sum of two second-rank tensors, assuming there is no rotation in the vertical plane,

$$\begin{pmatrix} E_{xx} & E_{xy} \\ E_{yx} & E_{yy} \end{pmatrix} + \begin{pmatrix} 0 & W_{xy} \\ -W_{yx} & 0 \end{pmatrix}$$

where the strain rate tensor is given by

$$E_{ij} = 0.5 \left(\frac{dU_i}{dj} + \frac{dU_j}{di} \right)$$

and the vorticity tensor is

$$W_{ij} = 0.5 \left(\frac{dU_i}{dj} - \frac{dU_j}{di} \right)$$

and Ui is the velocity in the i direction. The vertical strain rate is derived from the incompressibility of ice and the sum of the two principal surface strain rates: $E_{zz} = - (E_{xx} + E_{yy})$.

To obtain strain rates in an area, two methods were employed. Either strain rosettes or double lines of stakes were set out and surveyed twice; the second survey typically followed the initial survey after a year. In the case of strain rosettes, the strain rate is determined by assuming a linear velocity field between any three stakes in the rosette (usually the three outlying stakes). Velocities are measured relative to the central

stake, and are given by the horizontal change in position of the outer stakes divided by the time interval between surveys.

The velocity within the rosette is then expressed in the form,

$$U_x = A1x + A2y + A3$$

$$U_y = B1x + B2y + B3$$

where x and y are position coordinates and U_x and U_y are the velocity components in the x and y directions. The position and velocities are known for the three outlying stakes so the constants A1 to B3 can be determined from solving a set of simultaneous equations in the form,

$$\begin{pmatrix} x(a) & y(a) & 1 \\ x(b) & y(b) & 1 \\ x(c) & y(c) & 1 \end{pmatrix} \begin{pmatrix} A1 \\ A2 \\ A3 \end{pmatrix} = \begin{pmatrix} U_x(a) \\ U_x(b) \\ U_x(c) \end{pmatrix}$$

where the letters in parentheses denote the three outlying stakes. There is a similar expression for the components in the y direction. Assuming infinitesimal strain, the strain rates are then given by:

$$A1 = dU_x/dx = E_{xx}$$

$$B2 = dU_y/dy = E_{yy}$$

$$0.5(A2 + B1) = 0.5(dU_x/dy + dU_y/dx) = E_{xy}$$

where positive values denote extension and negative values denote compression.

For the double line of stakes, the first stage in calculating the strain rates is again to determine the velocity field. This is

done by solving an overdetermined set of time-dependent observation equations to derive, with error estimates, the position and velocity for each stake site, using the method described in Wager et al (1980). The position and velocity of the stakes are then used in a series of interconnecting triangles down the scheme using a different linear velocity field for each triangle.

Measurement Errors

A combination of field measurements of distances, angles and azimuths was made to determine strain rates. During the first field season, 1983-84, distances were measured by CA 1000 Telurometers and HP Electronic Distance Meters (EDM's), which are accurate to within 3 cm per 1500 m and 1 cm per 1500 m, respectively. Geodimeter 112 EDM's were used during the next two field seasons; accurate to $\pm$ 1 cm per 1500 m. The greater accuracy of the EDM's made their horizontal positions above the stake significant. The theodolite mounting of the EDM was optically plumbed onto the stake, so we consider a reasonable error to be 1 cm. However, where strain nets were measured using only distances the misclosure was more typically 2 cm.

The mean misclosure between rounds of the angle measurements was 4 seconds of arc. However, one of the instruments in the 1984-85 season consistently misclosed to 20 or 30 seconds of arc. In this case, measurements were repeated up to five times to obtain a consistent reading. In calculating the errors of the strain rate, a minimum error of 5 seconds of arc was used; if the misclosure was greater than 5 seconds, the size of the misclosure was taken as the value of the error.

Azimuths were measured with the least accuracy. The greatest contributions to the azimuth error were in the determinations of time and longitude. A 1-second error in time contributes to about a 15-second-of-arc error in azimuth; a 1-second error in longitude gives a 1-second-of-arc error in azimuth. Time was

taken from the satellite tracking unit, or from radio time signals. Sometimes wristwatches were used which were later calibrated using a satellite tracking unit. We have not calibrated the time given by these units, but we note that when they have been run concurrently they can differ in time by up to 1 second. Therefore, we have used an error of 1 second for time.

The position in longitude is known to better than 1 minute when a geoceiver position is used, but when single SATNAV fixes are used the longitude error could be up to 10 minutes of arc. SATNAV satellite receivers (Racal-Decca 412) are a single-channel system accurate to $\pm$200 m after about 5 passes, and were used in the place of the MX1502 geoceivers during the 1983-84 field season. Only a few station positions have been estimated by one SATNAV position; the remainder are determined using either three SATNAV fixes or up to 50 geoceiver fixes. We have used 45 seconds of arc as the error in azimuth. This may be high for azimuths measured under optimum conditions: where time is taken directly from a geoceiver using a stopwatch to measure lapse time, and longitude is taken from a geoceiver position. Figure 4 and Table 3 present the strain rate data.

ORIGINAL PAGE IS
OF POOR QUALITY

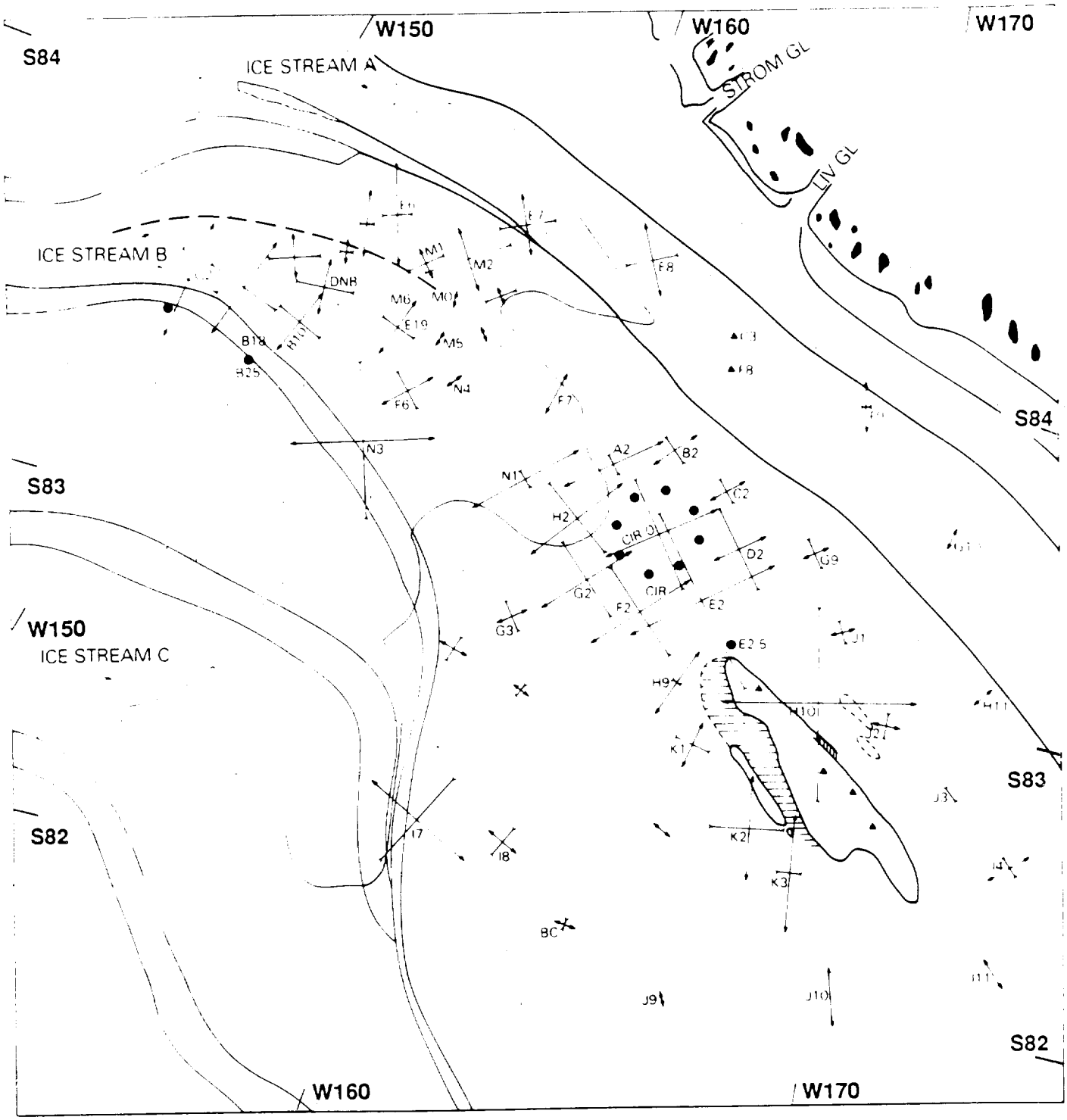

Figure 4: Regional map showing selected strain rates.

TABLE 3: STRAIN RATES

STATION	P1* $x10^{-3}a^{-1}$	P2* $x10^{-3}a^{-1}$	PZ** $x10^{-3}a^{-1}$	ROTATION+ $x10^{-3}$rad/a	BEARING of P1	DATE
CRARY						
A1	4.04 ± 0.01	-2.93 ± 0.01	-1.11 ± 0.02	0.4 ± 0.2	45.98 ± 0.06	83,84
A2	3.79 ± 0.02	-0.59 ± 0.02	-3.20 ± 0.03	1.9 ± 0.2	50.4 ± 0.1	84,85
B1	3.03 0.02	-2.38 0.02	-0.65 0.03	1.5 0.2	47.2 0.1	83,84
B2	1.79 0.02	-0.97 0.02	-0.82 0.03	0.7 0.2	42.7 0.3	83,84
C1	3.16 0.02	-2.66 0.02	-0.50 0.03	-0.6 0.2	54.0 0.1	83,84
C2	1.53 0.02	-0.87 0.02	-0.66 0.03	1.1 0.2	49.4 0.3	83,84
C2	1.53 0.02	-0.82 0.02	-0.71 0.02	-0.6 0.2	50.6 0.2	84,85
C3	0.04 0.02	-0.03 0.02	-0.01 0.03	-5.7 0.2	81 11	84,85
D1	3.50 0.03	-3.98 0.02	0.48 0.04	6.1 0.2	54.4 0.1	83,84
D2	1.97 0.02	-2.93 0.02	0.95 0.03	21.6 0.2	53.0 0.2	83,84
E1	5.27 0.04	-4.64 0.04	-0.63 0.05	1.8 0.2	50.6 0.1	83,84
E2	5.49 0.02	-6.68 0.02	1.19 0.02	2.0 0.2	51.71 0.04	83,84
E2.3	9.12 0.05	-7.19 0.06	-1.93 0.08	-4.0 0.2	74.6 0.1	84,85
E2.5	9.77 0.02	-11.88 0.02	2.11 0.02	3.8 0.2	60.69 0.02	84,85
E3	0.48 0.01	-0.05 0.03	-0.43 0.04	0.2 0.2	90 2	84,85
E4	0.28 0.08	0.05 0.06	-0.34 0.10	0.0 0.2	344.9 5	84,85
E'1	4.29 0.05	-4.39 0.05	0.10 0.07	-1.2 0.2	70.3 0.2	83,84
E'2	5.25 0.03	-4.34 0.03	-0.91 0.04	0.5 0.2	60.01 0.09	83,84
F1	5.34 0.02	-5.13 0.02	-0.21 0.03	-1.5 0.1	46.98 0.07	83,84
F2	4.13 0.02	-3.74 0.02	-0.39 0.03	1.8 0.2	43.7 0.1	83,84
G1	5.50 0.02	-5.80 0.02	0.29 0.03	4.5 0.2	45.22 0.05	83,84
G2	3.76 0.02	-3.06 0.02	-0.70 0.02	2.3 0.2	41.72 0.07	83,84
G2	3.74 0.01	-3.03 0.01	-0.70 0.02	2.0 0.2	41.70 0.05	84,85
G3	1.03 0.03	-1.03 0.02	-0.00 0.02	1.3 0.2	51.1 0.3	84,85
G4	0.99 0.09	-0.83 0.06	-0.2 0.1	1.8 0.1	102 2	84,85
H1	4.06 0.02	-3.48 0.02	-0.58 0.03	2.9 0.2	49.3 0.1	83,84
H2	4.15 0.02	-3.06 0.02	-1.09 0.02	-0.3 0.2	36.6 0.1	83,84
J1	0.90 0.02	-0.75 0.02	-0.15 0.03	3.2 0.2	68.6 0.5	84,85
J2	0.87 0.05	-0.83 0.05	-0.04 0.07	4.4 0.2	95 1	84,85
J3	0.14 0.02	+0.52 0.02	-0.66 0.03	3.0 0.2	48 1	84,85
K1	1.71 0.02	-1.23 0.02	-0.47 0.02	-1.7 0.2	13.0 0.2	84,85
K2	3.67 0.07	-2.27 0.06	-1.40 0.09	-4.9 0.2	353.7 0.5	84,85
K3	4.25 0.01	-0.78 0.03	-3.47 0.03	-6.3 0.2	357.3 0.2	84,85
LP1	0.22 0.02	0.00 0.02	-0.22 0.03	-0.1 0.1	49 2	84,85
O	4.44 0.04	-4.05 0.04	-0.39 0.05	1.5 0.2	53.5 0.1	83,84
O	4.57 0.04	-4.09 0.04	-0.48 0.06	1.8 0.2	53.3 0.1	84,85
DOWNSTREAM B						
A11	0.90 0.02	-0.42 0.03	-0.48 0.03	1.4 0.2	162.6 0.6	83,84
A19	2.56 0.02	-0.47 0.04	-2.08 0.04	1.4 0.2	162.7 0.3	83,84
A19	2.40 0.03	-0.39 0.03	-2.01 0.03	1.5 0.2	161.8 0.3	84,85
B10	2.63 0.02	-1.75 0.03	-0.88 0.03	5.0 0.2	194.9 0.2	83,84
B18	10.70 0.02	-6.06 0.02	-4.65 0.03	-8.6 0.2	53.09 0.03	84,85
B25	2.20 0.10	0.10 0.03	-2.30 0.03	0.9 0.2	97.3 0.4	84,85
C10	1.63 0.03	-1.92 0.03	0.29 0.04	16.9 0.2	149.4 0.3	83,84
E19	2.31 0.02	-1.32 0.04	-0.99 0.04	2.0 0.2	193.2 0.3	83,84
G1	3.95 0.01	-1.73 0.02	-2.22 0.02	3.9 0.2	188.1 0.1	84,85
G2	4.33 0.01	-2.17 0.02	-2.17 0.02	3.2 0.2	174.6 0.1	84,85
H2	1.17 0.02	0.88 0.02	-0.30 0.02	1.5 0.2	35.3 0.3	84,85
DNB	1.90 0.05	-1.96 0.03	0.06 0.06	1.8 0.2	165.1 0.3	83,84
DNB	2.05 0.09	-2.0 0.1	0.1 0.1	2.1 0.2	167.0 0.9	84,85
MO	0.48 0.02	-0.20 0.02	-0.28 0.03	0.5 0.2	171 1	84,85
M1	0.96 0.01	-1.17 0.01	0.21 0.02	0.6 0.2	137.8 0.2	84,85
M2	2.32 0.02	-3.12 0.02	0.79 0.03	2.7 0.2	141.7 0.1	84,85
M3	0.59 0.04	-1.08 0.05	0.49 0.06	1.0 0.2	140.4 0.8	84,85
M4	0.32 0.02	-0.17 0.02	-0.14 0.02	0.4 0.2	158 1	84,85
M5	0.52 0.03	-0.23 0.05	-0.29 0.05	1.4 0.2	186 1	84,85
M6	0.52 0.02	-0.68 0.02	0.16 0.02	1.4 0.2	172.2 0.6	84,85
N1	4.27 0.06	-0.54 0.06	3.73 0.08	8.2	43.9	85
N3	5.11 0.07	-5.46 0.05	-0.35 0.07	-17.9	65.8	85
N4	0.56 0.05	-0.22 0.06	0.34 0.07	0.1	35.1	85

*P1, P2= Principal axes of horizontal tension and compression, respectively.

**PZ= -(P1+P2), vertical strain rate.

+Rotation is clockwise, and bearing is clockwise from true North.

SECTION 3: SURFACE ELEVATIONS FROM GEOCEIVER AND OPTICAL LEVELLING

The Doppler satellite tracking system also provided measurements of surface elevation with respect to the reference ellipsoid WGS 72. This ellipsoid has a semi-major axis of 6378135 m and a flattening of 1/298.26 . Table 4 gives the measured elevation with each position determination. At 24 stations the elevation was measured twice; in 21 cases, the agreement was 8 m or less. Again, the standard deviation of elevation provided by the MX1502 decreased as the number of passes increased in the same manner as for the horizontal position. Seventy-five percent of the differences were within one standard deviation of the least accurate of the two elevations, and no differences were more than two standard deviations of the least accurate elevation.

Optical levelling was also carried out to gain detailed profiles of the ice surface. The distance between the level rod and optical level varied from 150 to 250 m. In early surveys, distances were estimated by Skidoo odometer; some were remeasured using EDM's as part of the strain-rate survey. During later surveys, upper and lower cross hairs were read which gave the distance between level rod positions and also served as a check on errors. Level lines were not closed. On three occasions, optical levelling was carried out between stations which had elevations that were also determined by geoceiver. The difference in elevation determined by each method typically misclosed by 2 to 3 m. This misclosure is fully accounted for by the error in the geoceiver-determined height and is consistent with the given errors. Table 5 gives geographic position of each profile; Table 6 gives the data. Figure 5 shows the geographic locations of each levelling line and Figure 6 presents the elevation profiles for these lines.

TABLE 4: ELEVATIONS FROM GEOCEIVER MEASUREMENTS

Station	Elevation (m)		Number of Passes		Difference (m)	Error (m)	Diff/Error
	YR1	YR2	YR1	YR2			
Crary							
E3	58	45	6	30	13	8	1.6
E4	64	66	15	7	2	8	
K1	26	20	5	8	6	10	
K2	18	18	7	8	0	9	
K3	8	4	13	4	4	10	
J1	31	37	6	11	6	9	
J2	26	31	3	15	5	11	
J3	32	29	18	16	3	6	
C4	177	212	1	14	34	18	1.8
G3	29	33	5	9	4	10	
G4	25	33	2	20	8	14	
L1	60	59	25	40	1	5	
LP1	98	94	9	20	4	7	
E2.3A	40	45	17	9	5	7	
O	36	44	8	10	8	8	1.0
A2		48		58			
C2		45		7			
C3		56		47			
G2		39		12			
H2		50		25			
Downstream B							
MO	74	81	12	23	7	6	1.2
E19	88	85	5	38	3	8	
DNB	91	90	45	23	1	5	
G1	114	133	5	4	19	12	1.6
G2	135	134	17	11	1	7	
A19	100	101	15	20	1	6	
B18	84	87	12	23	3	6	
B25	103	96	4	23	7	9	
H2	125	118	19	38	7	5	1.4
M2		70					
M3		56		34			
N1		49		8			
N2		52		27			
N3		47		28			
N4		70		7			
Downstream C							
DNC		99		25			
A1		91		24			
A2		86		6			
A3		74		15			
B2		64		15			
B3		123		??			
C1		116		16			
C3		125		8			
D19		30		45			
H5		50		8			
Wisconsin							
W9		61		22			
W6		50		23			
W5		59		5			
W3		94		20			

TABLE 5: POSITIONS OF OPTICALLY LEVELLED TRAVERSES

Station From->To	Line (Fig. 5)	Start Position LAT d m s	Start Position LONG d m s	End Position LAT d m s	End Position LONG d m s	Dist (km)	Bearing (deg)
CRARY							
A2->H2	2	83 57 37	164 14 14	83 53 17	164 02 45	8.22	15.8
A2->N1	6	83 57 37	164 14 14	83 55 15	163 29 24	10.07	63.8
E2.3A-E2.5	12	83 33 09	168 12 43	83 30 04	168 39 35	8.0	315.3
E2.3A-E2	13	83 33 09	168 12 43	83 36 43	167 40 53	9.0	135.3
E2.2->N	14	83 34 30	168 00 50	83 31 50	167 36 58	7.0	45.3
E2.2->S	15	83 34 30	168 00 50	83 35 38	168 11 07	3.0	225.3
E2.3A->S	16	83 33 09	168 12 43	83 35 14	168 31 38	5.5	225.3
E2.3A->N	17	83 33 09	168 12 43	83 30 29	167 48 56	7.0	45.3
E2.4->S	18	83 31 48	168 24 32	83 33 19	168 38 14	4.0	225.3
E2.4->N	19	83 31 48	168 24 32	83 31 14	168 19 26	1.5	45.3
L1(W)-L1(X)	20	83 06 11	172 25 20	83 06 25	172 24 44	0.5	162.4
L1(X)-L1(Z)	21	83 06 25	172 24 44	83 06 50	172 30 14	1.5	237.8
L1(Z)-L1(D)	22	83 06 50	172 30 14	83 08 05	172 44 02	3.8	232.8
O->C2	23	83 47 14	166 01 28	83 54 38	167 07 59	19.0	223.4
O->D1	24	83 47 14	166 01 28	83 47 33	166 56 21	11.0	266.5
DOWNSTREAM B							
E10-C10	1	84 10 44	155 37 12	84 12 53	153 06 35	28.49	99.3
A19-B10	3	84 24 27	154 42 21	84 02 42	154 07 06	40.99	0.0
N1-N1'	4	83 50 30	161 56 00	83 49 44	161 37 37	3.92	68.9
N1'-N4	5	83 49 44	161 37 37	84 03 44	159 01 17	40.08	131.6
E5->S	7	84 11 30	154 59 30	84 15 04	155 18 29	7.5	208.0
E5->N	8	84 11 30	154 59 30	84 07 53	154 41 31	7.5	27.0
C4->N	9	84 12 31	153 51 48	84 11 19	153 45 32	2.5	27.9
C4->S	10	84 12 31	153 51 48	84 16 20	154 12 07	8.0	207.9
C4(S16)->S	11	84 16 20	154 12 07	84 17 15	154 17 52	2.0	212.0
G2-G2'	25	84 00 28	150 32 03	83 58 26	149 39 14	13.0	70.2
B10-B18	34	84 02 42	154 07 06	83 57 00	153 33 18	12.62	32.1
DOWNSTREAM C							
O->A1	26	82 49 18	152 26 55	82 54 42	152 27 55	10.0	181.3
A3->O	27	83 18 42	152 32 05	83 16 00	152 31 38	5.0	1.1
O-B3	28	82 49 18	152 26 55	82 18 07	152 23 07	59.5	0.9
O->D19	29	82 49 18	152 26 55	82 49 09	154 25 51	27.5	269.6
D19->O	30	82 48 55	155 17 34	82 49 08	154 25 43	12.0	92.4
B27-H5	31	82 34 42	152 25 09	82 35 26	153 15 05	12.0	263.1
A4-H5	32	82 37 41	153 03 22	82 35 26	153 15 05	5.0	326.2
H5-B2	33	82 35 26	153 15 05	82 34 32	153 19 44	2.0	326.2

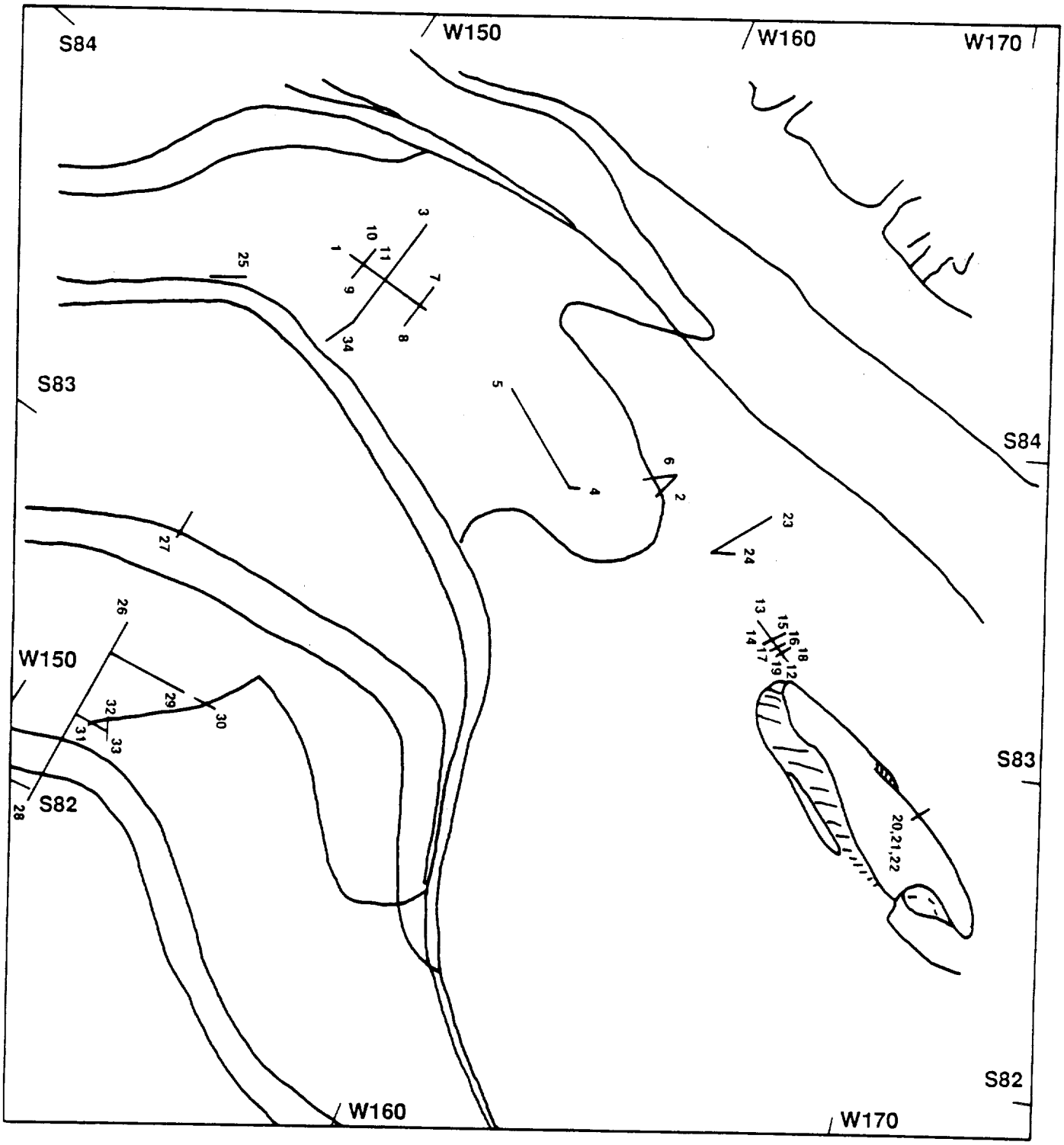

Figure 5: Regional map showing lines of optical levelling.

TABLE 6: SURFACE ELEVATION PROFILES FROM OPTICAL LEVELLING

LINE 1
DNB
E10 to C10

Dist (km)	El (m)
0.00	136.99
0.48	137.38
0.96	138.10
1.44	138.95
1.91	139.66
2.39	140.00
2.86	140.28
3.34	140.30
3.81	140.72
4.29	141.21
4.77	141.69
5.24	142.11
5.72	142.43
6.21	142.81
6.70	142.78
7.19	142.82
7.67	142.85
8.14	142.51
8.62	142.31
9.11	142.08
9.60	142.19
10.09	142.24
10.59	142.27
11.10	142.32
11.60	141.95
12.07	141.56
12.54	141.07
13.01	140.20
13.48	139.62
13.96	139.24
14.43	139.00
15.02	138.91
15.60	139.42
16.08	140.26
16.57	141.50
17.05	142.43
17.53	143.02
18.02	143.50
18.50	143.68
18.98	143.74
19.47	143.65
19.95	143.20
20.43	143.02
20.91	142.79
21.39	142.52
21.88	142.21
22.37	141.80
22.86	141.32
23.33	140.89
23.79	139.97
24.26	138.97
24.72	138.26
25.18	137.34
25.64	136.83
26.13	136.76
26.62	136.73
27.11	136.82
27.57	136.64
28.03	136.32
28.49	136.09

LINE 2
CIR
A2 toward H2

Dist(km)	El(m)
0.000	91
0.392	91.82
0.736	92.27
1.092	92.16
1.440	92.05
1.732	92.05
2.091	91.72
2.383	91.14
2.735	90.77
3.099	91.02
3.463	91.34
3.825	91.00
4.114	91.08
4.514	91.19
4.880	92.34
5.222	93.76
5.532	94.66
5.892	95.63
6.229	96.13
6.614	96.28
7.007	96.03
7.413	95.99
7.738	95.60
8.017	95.75
8.220	95.77

LINE 3
DNB
A19 to B10

Dist (km)	El (m)
0.00	150.00
0.50	149.52
1.00	148.01
1.40	147.19
1.90	146.91
2.40	145.57
2.90	145.13
3.40	145.10
3.90	146.53
4.30	146.78
4.80	145.33
5.30	143.80
5.80	140.49
6.30	138.12
6.80	135.30
7.20	133.88
7.70	134.46
8.20	135.42
8.70	135.25
9.20	135.20
9.70	136.48
10.10	138.79
10.60	140.76
11.10	141.70
11.60	141.39
12.10	139.97
12.50	137.50
13.00	142.23
13.50	143.92
14.00	144.05
14.50	143.65
14.90	144.03
15.40	144.74
15.90	146.33
16.40	143.19
16.90	142.85
17.40	144.95
17.80	146.84
18.32	148.33
18.84	148.08
19.36	146.28
19.85	147.25
20.34	149.23
20.83	150.14
21.29	149.16
21.74	147.59
22.20	145.94
22.67	144.21
23.14	142.09
23.61	139.47
24.10	138.03
24.58	138.80
25.06	139.47
25.51	138.51
25.96	137.32
26.41	135.97
27.09	135.91
27.37	136.00
27.86	136.34
28.36	136.97
28.87	137.02
29.38	137.47
29.87	138.44
30.35	139.92
30.83	141.59
31.32	143.58
31.80	145.11
32.29	145.35
32.78	144.44

33.27	144.45
33.76	144.41
34.25	144.09
34.74	145.04
35.23	146.94
35.71	147.89
36.20	147.86
36.68	146.69
37.15	146.23
37.62	144.62
38.08	142.61
38.56	140.66
39.03	141.33
39.51	143.00
40.00	143.61
40.49	144.26
40.99	143.93

LINE 4
DNB
N1 to N1'

Dist (km)	El (m)
0.000	92
0.367	92.37
0.746	93.29
1.186	94.50
1.626	95.29
2.056	96.54
2.458	98.09
2.860	99.93
3.260	101.37
3.690	102.29
3.922	102.46

LINE 5
DNB
N1' to N4

Dist(km)	El(m)
0.000	102.46
0.347	102.28
0.672	102.24
1.048	102.36
1.410	102.47
1.718	102.94
2.074	103.68
2.449	104.65
2.805	105.03
3.162	105.25
3.597	105.36
4.000	105.27
4.371	105.66
4.732	106.05
5.063	106.50
5.484	107.03
5.819	107.47
6.241	108.07
6.606	108.79
6.986	109.97
7.398	111.10
7.792	111.79
8.224	112.40
8.606	112.92
8.982	112.85
9.360	112.65
9.729	112.93
10.132	113.38
10.538	113.48
10.933	113.73
11.320	114.07
11.724	114.78
12.099	115.36
12.546	115.71
12.926	115.54
13.377	115.29
13.782	115.03
14.208	115.36
14.600	115.70
14.981	116.15
15.427	116.82
15.809	117.18
16.285	119.10
16.665	120.24
17.102	121.21
17.512	122.40
17.937	123.67
18.345	124.79
18.780	125.87
19.160	126.66
19.598	127.26

19.959	127.55
20.340	127.48
20.756	127.15
21.139	126.19
21.532	125.14
21.921	123.94
22.288	122.83
22.675	121.78
23.058	121.08
23.424	120.51
23.769	120.24
24.164	120.23
24.539	120.51
24.906	120.70
25.320	120.77
25.787	120.84
26.270	120.69
26.646	120.42
27.058	120.36
27.431	120.30
27.735	120.46
28.110	120.37
28.462	120.36
28.848	120.28
29.191	120.24
29.580	120.07
29.917	120.02
30.357	119.91
30.689	119.52
31.040	119.13
31.394	118.67
31.788	117.81
32.102	117.15
32.425	116.50
32.736	115.79
33.125	115.12
33.471	114.65
33.885	114.18
34.254	113.80
34.630	113.54
34.993	113.42
35.357	113.41
35.686	113.16
36.065	112.83
36.462	112.63
36.890	112.50
37.256	112.52
37.638	112.61
37.995	112.79
38.378	113.05
38.740	113.43
39.070	114.00
39.451	114.37
39.788	114.85
40.084	114.82

LINE 6
CIR
A2 toward N1

Dist(km)	El(m)
0.000	91.00
0.413	91.90
0.767	92.32
1.065	92.38
1.401	92.50
1.752	92.13
2.101	91.87
2.456	91.57
2.754	91.33
3.094	91.19
3.456	91.62
3.794	92.49
4.142	94.11
4.459	95.27
4.787	96.31
5.135	96.31
5.497	96.12
5.837	96.43
6.193	97.45
6.543	97.35
6.833	94.15
7.122	93.08
7.434	93.32
7.771	95.49
8.125	96.61
8.420	94.26
8.717	93.71
9.046	95.24
9.378	96.37
9.716	97.20
10.071	97.60

LINE 7
DNB
E5 to E5(S15)

0.0	142.82
0.5	142.74
1.0	143.06
1.5	143.68
2.0	144.12
2.5	143.93
3.0	142.63
3.5	139.90
4.0	139.69
4.5	140.88
5.0	141.54
5.5	141.08
6.0	139.92
6.5	138.54
7.0	138.34
7.5	138.67

LINE 8
DNB
E5 to E5(N15)

0.0	142.82
0.5	143.45
1.0	143.64
1.5	142.91
2.0	142.27
2.5	141.20
3.0	139.41
3.5	138.26
4.0	138.32
4.5	138.89
5.0	138.73
5.5	138.99
6.0	140.57
6.5	143.11
7.0	143.60
7.5	141.98

LINE 9
DNB
C4 to C4(N5)

0.0	143.20
0.5	141.56
1.0	140.52
1.5	139.40
2.0	138.89
2.5	139.36

LINE 10
DNB
C4 to C4(S16)

Dist(km)	El (m)
0.0	143.20
0.5	143.66
1.0	142.79
1.5	141.29
2.0	138.99
2.5	135.00
3.0	134.33
4.0	133.80
4.5	133.74
5.0	134.14
5.5	134.23
6.0	135.22
6.5	138.44
7.0	140.71
7.5	139.91
8.0	139.43

LINE 11
DNB
C4(S16) to C4(S20)

Dist(km)	El(m)
0.00	139.43
0.5	139.91
1.0	140.87
1.5	141.04
2.0	139.85

LINE 12
CIR
E2.3A to E2.5

Dist(km)	El(m)
0.00	83
0.5	81.37
1.0	79.83
1.5	79.67
2.0	78.85
2.5	76.31
3.0	74.13
3.25	71.95
3.5	71.14
4.0	71.34
4.5	72.32
5.0	72.96
5.5	73.74
6.0	74.16
6.5	72.64
7.0	72.83
7.5	74.48
8.0	75.57

LINE 13
CIR
E2.3A to E2

Dist(km)	El(m)
0.0	83
0.5	83.33
1.0	82.67
1.5	83.55
2.0	85.09
2.5	86.00
3.0	87.28
3.5	87.21
4.0	86.64
4.5	86.27
5.0	85.54
5.5	85.66
6.0	85.66
6.5	85.04
7.0	85.35
7.5	84.77
8.0	82.81
8.5	80.45
9.0	80.04

LINE 14
CIR
E2.2 to E2.2(N)

Dist(km)	El(m)
0.0	87.21
0.5	86.53
1.0	85.94
1.5	85.35
2.0	85.59
2.5	85.18
3.0	84.89
3.5	84.86
4.0	84.23
4.5	86.32
5.0	87.06
5.5	86.54
6.0	85.89
6.5	85.43
7.0	81.53

LINE 15
CIR
E2.2 to E2.2(S)

Dist(km)	El(m)
0.0	87.21
0.5	86.64
1.0	85.51
1.5	81.81
2.0	82.56
2.5	83.48
3.0	82.96

LINE 16
CIR
E2.3A to E2.3A(S)

Dist(km)	El (m)
0.0	83
0.5	84.20
1.0	83.33
1.5	82.86
2.0	82.38
2.5	82.28
3.0	81.55
3.5	80.95
4.0	80.10
4.5	78.49
5.0	78.83
5.5	77.72

LINE 17
CIR
E2.3A to E2.3A(N)

Dist(km)	El(m)
0.0	83
0.5	80.84
1.0	81.40
1.5	83.31
2.0	84.43
2.5	84.74
3.0	85.18
3.5	85.85
4.0	87.48
4.5	87.95
5.0	88.53
5.5	87.75
6.0	85.53
6.5	84.01
7.0	82.68

LINE 18
CIR
E2.4 to E2.4(S)

Dist(km)	El(m)
0.0	71.14
0.5	72.20
1.0	71.68
1.5	72.13
2.0	73.48
2.5	74.05
3.0	73.53
3.5	74.19
4.0	74.45

LINE 19
CIR
E2.4 to E2.4(N)

Dist(km)	El(m)
0.0	71.14
0.5	71.49
1.0	71.89
1.5	70.72

LINE 20
CIR
L1(W) to L1(X)

Dist(m)	El(m)
0.00	102
334.30	99.855
450.47	99.083

LINE 21
CIR
L1(X) to L1(Z)

Dist(m)	El(m)
0.00	99.083
101.40	97.905
317.50	95.213
512.70	92.562
730.50	89.189
898.60	86.525
1126.40	82.789
1276.60	79.974
1402.30	77.377
1447.70	76.154

LINE 22
CIR
L1(Z) to L1(D)

Dist(m)	El(m)
0.00	76.154
86.30	74.191
208.20	71.527
363.10	68.803
479.80	67.033
687.60	65.066
838.10	62.503
1014.80	61.740
1217.10	61.445
1433.10	60.725
1639.10	60.845
1858.10	60.675
2075.10	60.465
2345.10	60.015
2567.10	59.765
2846.10	59.475
3068.10	59.465
3367.10	59.355
3633.10	59.285
3817.40	59.100

LINE 23
CIR
O toward C2

Dist(km)	El(m)
0.00	87
0.25	88.02
0.50	88.46
0.75	88.69
1.00	88.60
1.25	89.26
1.50	89.81
1.75	89.90
2.00	89.85
2.25	90.10
2.50	90.09
2.75	90.03
3.00	90.33
3.25	90.95
3.50	91.19
3.75	91.01
4.00	91.14
4.25	91.14
4.50	91.54
4.75	91.77
5.00	92.06
5.25	92.23
5.50	91.62
5.75	90.82
6.00	90.09
6.25	89.58
6.50	89.42
7.00	89.10
7.25	88.62
7.50	88.01
7.75	88.13
8.00	89.00
8.25	89.67
8.50	89.82
8.75	89.92
9.00	89.88
9.25	89.45
9.50	89.85
9.75	89.99
10.00	90.59
10.25	91.29
10.50	91.54
10.75	91.52
11.00	91.54
11.25	91.56
11.50	91.69
11.75	91.71
12.00	91.76
12.25	91.82
12.50	91.80
12.75	91.84
13.00	91.86
13.25	91.82
13.50	91.58
13.75	91.91
14.00	91.69
14.25	91.75
14.50	91.78
14.75	91.89
15.00	92.06
15.25	91.97
15.50	92.09
15.75	92.05
16.00	92.05
16.25	91.86
16.50	91.49
16.75	90.88
17.00	90.37
17.25	90.61

17.50	91.59
17.75	91.94
18.00	92.04
18.25	92.20
18.50	92.05
18.75	92.21
19.00	92.11

LINE 24
CIR
0 toward D1

Dist(km)	El(m)
0.00	87
0.25	87.56
0.50	87.73
0.75	87.85
1.00	87.85
1.25	87.85
1.50	87.83
1.75	88.38
2.00	89.01
2.25	87.39
2.50	87.89
2.75	88.19
3.00	88.09
3.25	87.94
3.50	87.81
3.75	87.64
4.00	87.43
4.25	87.55
4.50	87.68
4.75	87.91
5.00	87.92
5.25	87.84
5.50	87.89
5.75	88.14
6.00	88.60
6.25	89.02
6.50	89.25
6.75	89.25
7.00	89.22
7.25	89.25
7.50	89.30
7.75	89.30
8.00	89.28
8.25	89.05
8.50	88.35
8.75	87.82
9.00	86.85
9.25	86.14
9.50	86.39
9.75	86.84
10.00	86.92
10.25	87.04
10.50	86.70
10.75	86.22
11.00	85.78

LINE 25
DNB
G2 to G2'

Dist(km)	El(m)
0.0	178
0.5	178.74
1.0	179.42
1.5	180.00
2.0	179.86
2.5	179.18
3.0	177.99
3.5	177.09
4.0	176.65
4.5	176.17
5.0	175.70
5.5	175.51
6.0	175.20
6.5	175.28
7.0	176.34
7.5	177.77
8.0	179.26
8.5	180.80
9.0	181.94
9.5	183.31
10.0	184.61
10.5	185.69
11.0	186.43
11.5	187.69
12.0	188.71
12.5	190.17
13.0	191.65

LINE 26
DNC
O toward A1

Dist(km)	El(m)
0.00	142
0.25	142.11
0.50	141.96
0.75	141.38
1.00	141.06
1.25	140.74
1.50	140.54
1.75	140.19
2.00	139.80
2.25	139.41
2.50	139.36
2.75	139.38
3.00	139.11
3.25	138.85
3.50	138.58
3.75	138.66
4.00	138.88
4.25	138.60
4.50	138.20
4.75	137.90
5.00	137.81
5.25	137.84
5.50	137.79
5.75	137.71
6.00	137.53
6.25	137.39
6.50	137.11
6.75	137.14
7.00	137.05
7.25	136.66
7.50	136.15
7.75	135.56
8.00	135.26
8.25	135.14
8.50	135.18
8.75	135.13
9.00	134.95
9.25	135.13
9.50	135.42
9.75	135.60
10.00	135.57

LINE 27
DNC
A3 toward O

Dist(km)	El(m)
0.0	117
0.5	115.27
1.0	114.09
1.5	112.76
2.0	111.71
2.5	110.93
3.0	110.24
3.5	108.78
4.0	107.46
4.5	105.20
5.0	103.37

LINE 28
DNC
O to B3

Dist(km)	El(m)
0.00	142
0.25	141.91
0.50	141.76
0.75	141.82
1.00	141.83
1.25	141.92
1.50	142.21
1.75	142.63
2.00	142.83
2.25	143.56
2.50	145.46
2.75	146.79
3.00	147.13
3.25	146.98
3.50	147.21
3.75	147.72
4.00	148.24
4.25	148.29
4.50	148.50
4.75	148.65
5.00	148.52
5.25	148.36
5.50	148.04
5.75	148.10
6.00	148.34
6.25	148.64
6.50	148.77
6.75	148.80
7.00	148.55
7.25	148.17
7.50	147.45
7.75	146.79
8.00	146.43
8.25	146.02
8.50	145.33
8.75	144.40
9.00	143.71
9.25	143.42
9.50	142.62
9.75	142.11
10.00	141.85
10.25	141.74
10.50	141.65
10.75	141.56
11.00	141.21
11.25	141.07
11.50	140.57
11.75	140.52
12.00	140.37
12.25	140.29
12.50	139.99
12.75	139.61
13.00	139.50
13.25	139.31
13.50	139.27
13.75	139.22
14.00	139.22
14.25	139.64
14.50	139.86
14.75	140.33
15.00	140.53
15.25	140.57
15.50	140.83
15.75	140.91
16.00	141.19
16.25	141.54
16.50	141.48
16.75	141.69
17.00	141.92

17.25	142.31
17.50	142.72
17.75	143.05
18.00	143.45
18.25	143.94
18.50	144.24
18.75	144.61
19.00	144.71
19.25	144.61
19.50	144.04
19.75	143.48
20.00	143.34
20.25	143.19
20.50	143.29
20.75	143.48
21.00	143.70
21.25	143.95
21.50	144.17
21.75	144.32
22.00	144.66
22.25	144.87
22.50	144.86
22.75	144.66
23.00	144.64
23.25	144.68
23.50	144.82
23.75	144.83
24.00	144.54
24.25	144.17
24.50	143.99
24.75	144.18
25.00	144.22
25.25	143.75
25.50	143.01
25.75	142.00
26.00	141.24
26.25	140.44
26.50	139.17
26.75	138.40
27.00	136.80
27.25	135.42
27.50	134.13
27.75	132.75
28.00	131.22
28.25	129.49
28.50	127.84
28.75	126.49
29.00	124.45
29.25	123.00
29.50	121.20
29.75	119.06
30.00	117.30
30.5	114.65
31.0	112.04
31.5	110.23
32.0	108.94
32.5	107.82
33.0	107.31
33.5	106.20
34.0	105.51
34.5	104.87
35.0	104.41
35.5	104.29
36.0	104.92
36.5	106.12
37.0	107.70
37.5	109.26
38.0	110.50
38.5	111.46
39.0	111.95
39.5	111.52
40.0	111.21
40.5	111.54
41.0	112.29

41.5	114.81
42.0	114.84
42.5	114.44
43.0	114.16
43.5	115.53
44.0	117.92
44.5	120.21
45.0	125.91
45.5	129.51
46.0	132.19
46.5	134.86
47.0	138.06
47.5	141.30
48.0	144.81
48.5	148.23
49.0	151.43
49.5	155.16
50.0	159.13
50.5	162.08
51.0	164.03
51.5	165.55
52.0	166.85
52.5	167.56
53.0	168.30
53.5	168.76
54.0	169.08
54.5	169.31
55.0	168.91
55.5	168.22
58.0	167.84
58.5	167.72
59.5	166.60

LINE 29
DNC
O toward D19

Dist(km)	El(m)
0.00	142
0.25	141.75
0.50	141.34
0.75	140.99
1.00	140.45
1.25	140.09
1.50	139.69
1.75	139.33
2.00	139.07
2.25	138.77
2.50	138.22
2.75	137.81
3.00	137.50
3.25	137.09
3.50	136.50
3.75	136.01
4.00	135.51
4.25	135.05
4.50	134.59
4.75	134.13
5.00	133.78
5.25	132.78
5.50	132.98
6.00	132.13
6.50	131.18
7.0	130.56
7.5	130.19
8.0	129.60
8.5	128.94
9.0	128.81
9.5	127.44
10.0	126.97
10.5	126.72
11.0	126.33
11.5	126.06
12.0	125.75
12.5	125.49
13.0	125.11
13.5	124.72
14.0	124.28
14.5	123.83
15.0	123.09
15.5	122.48
16.0	121.56
16.5	120.89
17.0	120.45
17.5	119.77
18.0	119.38
18.5	118.35
19.0	117.72
19.5	116.98
20.0	116.30
20.5	116.09
21.0	115.58
21.5	115.32
22.0	115.14
22.5	114.88
23.0	114.56
23.5	114.20
24.0	113.93
24.5	113.57
25.0	112.92
25.5	112.13
26.0	111.02
26.5	109.93
27.0	109.21
27.5	109.09
28.0	109.04

LINE 30
DNC
D19 toward 0

Dist(km)	El(m)
0.0	73
0.5	73.86
1.0	73.04
1.5	71.16
2.0	73.85
2.5	82.94
3.0	89.78
3.5	95.04
4.0	98.01
4.5	100.01
5.0	101.49
5.5	103.57
6.0	104.52
6.5	104.98
7.0	105.45
7.5	105.57
8.0	105.92
8.5	106.27
9.0	106.68
9.5	107.09
10.0	107.30
10.5	107.37
11.0	107.24
11.5	107.14
12.0	107.16

LINE 31
DNC
B27 to H5

Dist(km)	El(m)
0.0	136.80
0.5	133.82
1.0	130.94
1.5	127.98
2.0	124.79
2.5	121.14
3.0	117.31
3.5	112.94
4.0	108.17
4.1	106.55
4.5	102.78
4.7	100.44
5.0	96.49
5.25	93.09
5.50	89.22
5.80	85.26
6.0	82.12
6.5	79.45
7.0	79.48
7.5	80.53
8.0	80.78
8.5	80.25
9.0	79.67
9.5	78.76
10.0	78.42
10.5	78.46
11.0	78.39
11.5	78.12
12.0	78.03

LINE 32
DNC
A4(RISP) to H5

Dist(km)	El(m)
0.0	115.84
0.25	112.36
0.5	108.38
0.7	105.18
0.9	101.71
1.0	99.87
1.145	97.03
1.425	93.31
1.656	90.03
1.829	87.36
2.0	85.66
2.5	86.60
3.0	87.11
3.5	86.02
4.0	85.10
4.5	85.26
5.0	85

LINE 33
DNC
H5-B2(RISP)

Dist(km)	El(m)
0.0	85
0.5	85.30
1.0	86.26
1.5	86.49
2.0	86.52

LINE 34
DNB
B10-B18

Dist(km)	El(m)
0.0	143.93
0.52	143.79
1.04	143.35
1.55	142.58
2.07	143.17
2.58	144.28
3.09	145.28
3.60	144.58
4.11	143.20
4.62	143.36
5.13	142.48
5.61	141.77
6.09	140.01
6.57	140.28
7.09	141.18
7.61	140.58
8.14	139.14
8.64	138.06
9.14	138.18
9.64	138.27
10.14	138.17
10.63	137.34
11.13	136.03
11.63	136.05
12.12	135.66
12.62	135.35

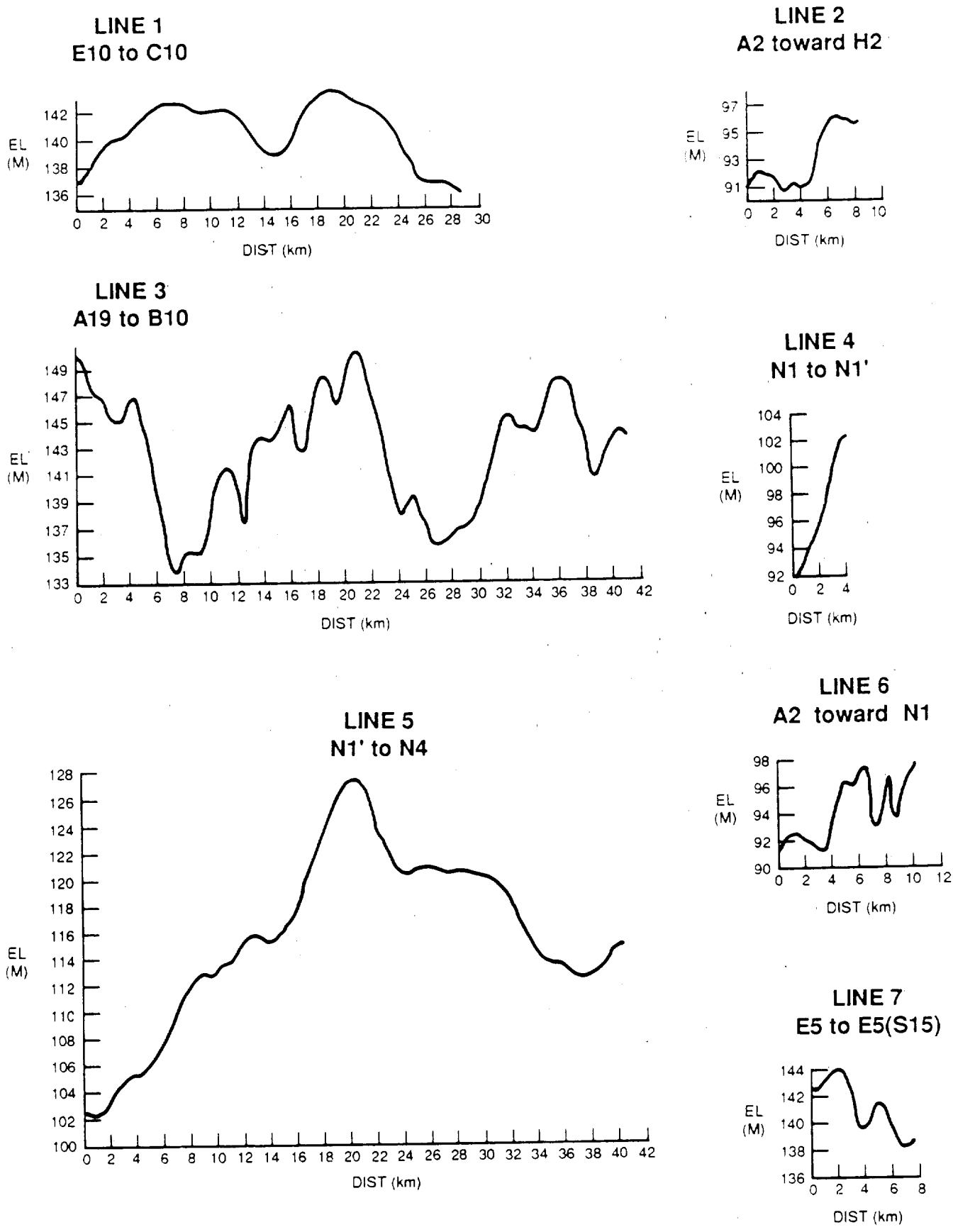

Figure 6: Elevation profiles from optical levelling.

LINE 8
E5 to E5(N15)

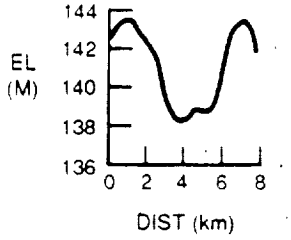

LINE 9
C4 to C4(N5)

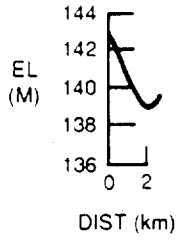

LINE 10
C4 to C4(S16)

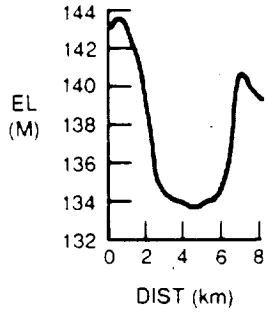

LINE 11
C4(S16) to C4(S20)

LINE 12
E2.3A to E2.5

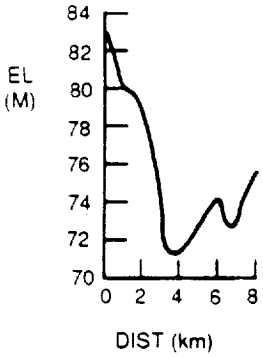

LINE 13
E2.3A to E2

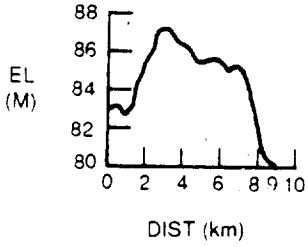

LINE 14
E2.2 to E2.2(N)

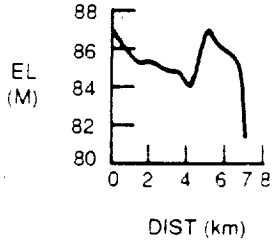

LINE 15
E2.2 to E2.2(S)

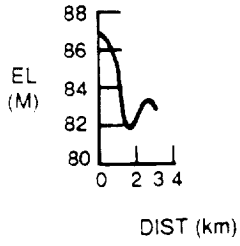

LINE 16
E2.3A to E2.3A(S)

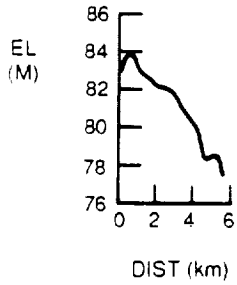

LINE 17
E2.3A to E2.3A(N)

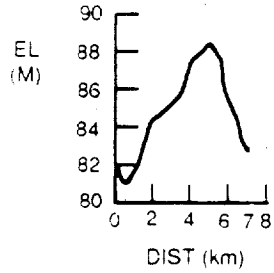

LINE 18
E2.4 to E2.4(S)

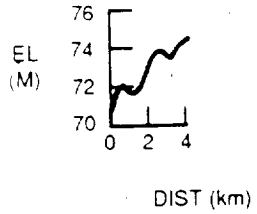

LINE 19
E2.4 to E2.4(N)

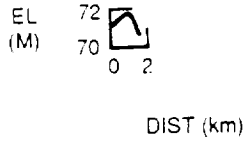

LINE 20
L1(W) to L1(X)

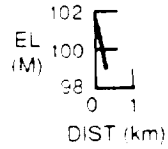

LINE 21
L1(X) to L1(Z)

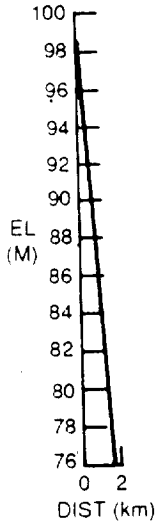

LINE 22
L1(Z) to L1(D)

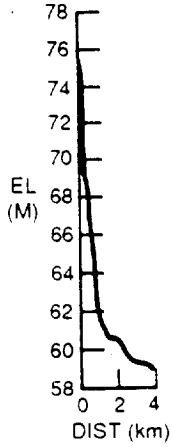

LINE 23
0 toward C2

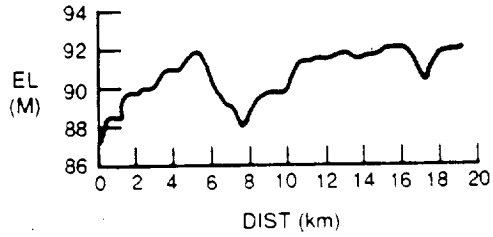

LINE 24
0 toward D1

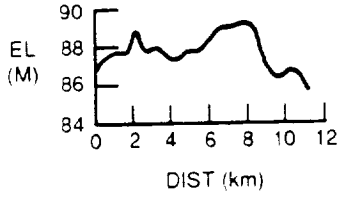

LINE 25
G2 to G2'

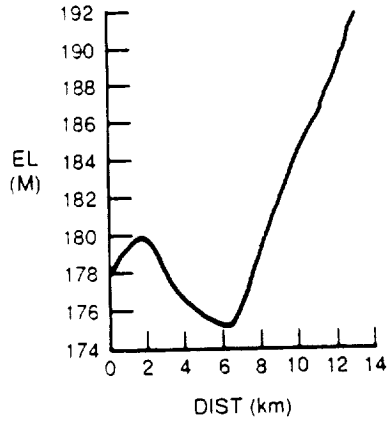

LINE 26
0 toward A1

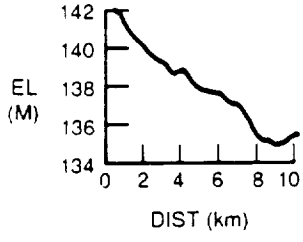

LINE 27
A3 toward 0

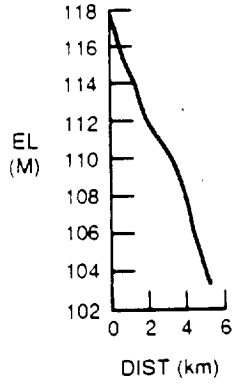

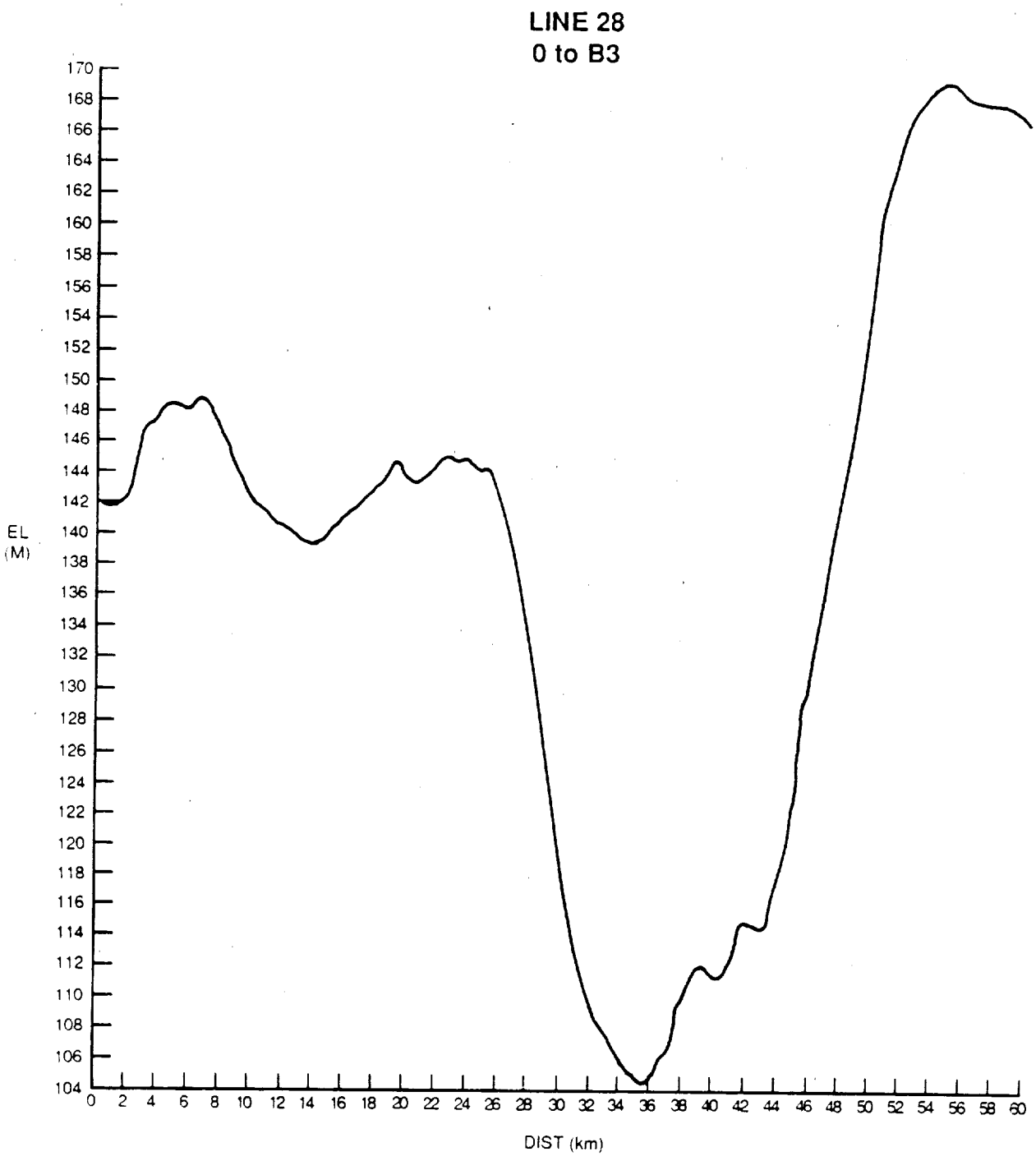
LINE 28
0 to B3
EL
(M)
170
168
166
164
162
160
158
156
154
152
150
148
146
144
142
140
138
136
134
132
130
128
126
124
122
120
118
116
114
112
110
108
106
104
0 2 4 6 8 10 12 14 16 18 20 22 24 26 28 30 32 34 36 38 40 42 44 46 48 50 52 54 56 58 60
DIST (km)

LINE 29
0 toward D19

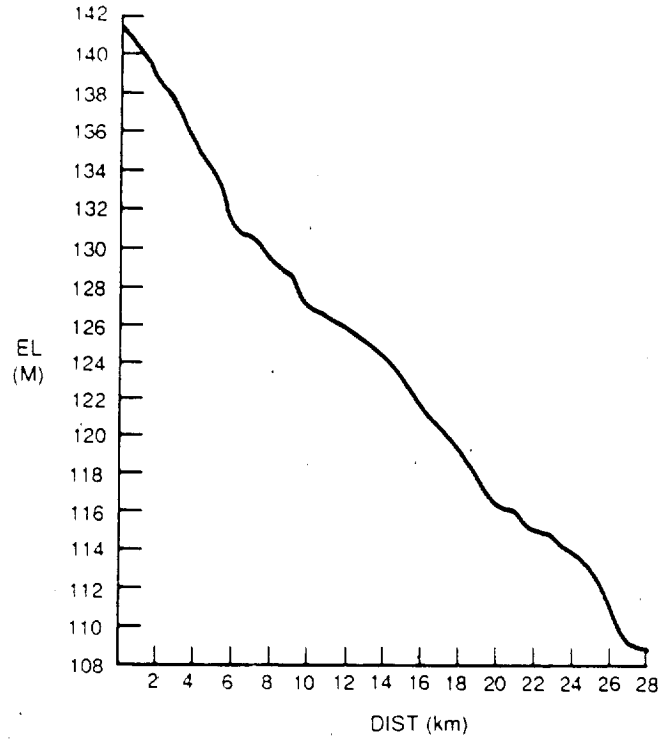

LINE 30
D19 toward 0

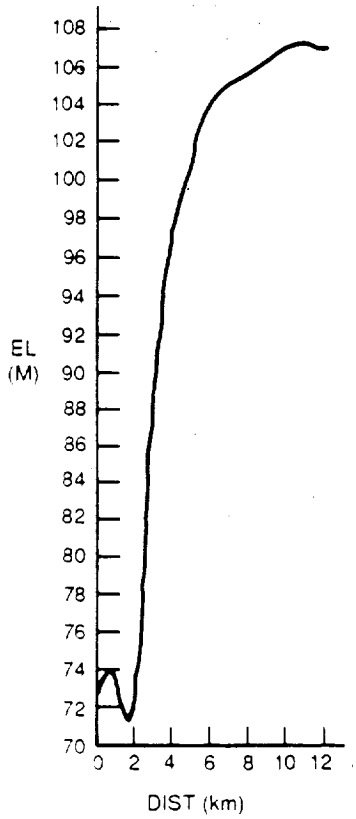

LINE 31
B27 to H5

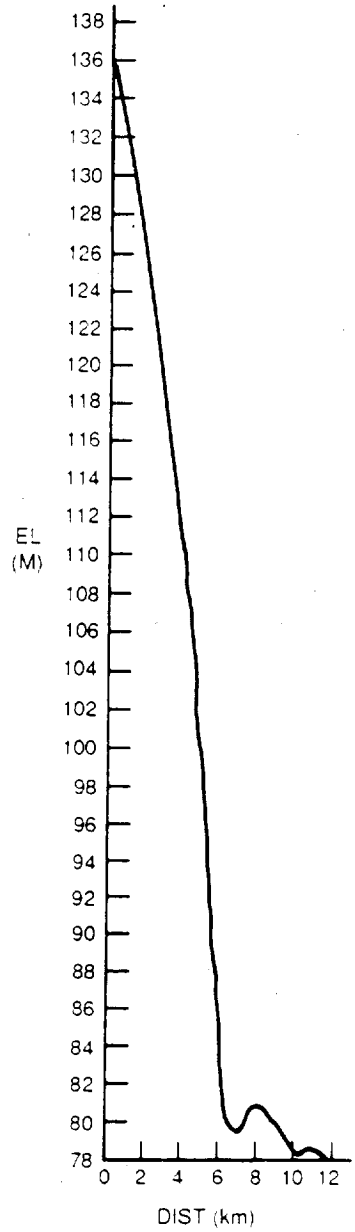

LINE 32
A4(RISP) to H5

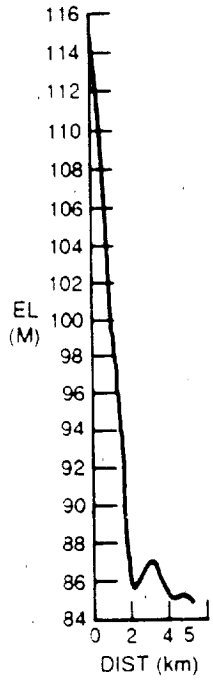

LINE 33
H5 to B2(RISP)

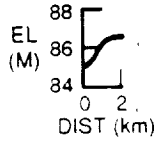

LINE 34
B10 to B18

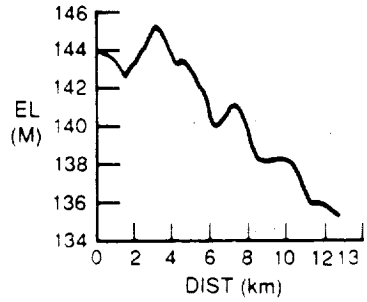

SECTION 4: RADIO-ECHO SOUNDING OF ICE THICKNESS

Spot measurements of ice thickness were made at several survey stations (Table 7) and along three short profiles near the grounding line of Ice Stream B (Tables 8, 9 and 10 and Figure 7). The radio-echo sounder used was on loan from the University of Wisconsin, Geophysics and Polar Science Center. A description of this radio-echo system is given by Shabtaie and Bentley (1987). To reduce the two-way travel time to ice thickness, a velocity of 169 $x10^{-6}$ m/s was used for the radar energy (Shabtaie, personal communication).

TABLE 7: STATION ICE THICKNESS

STATION	TWO-WAY TRAVEL TIME (μs)	THICKNESS (m)
M2	8.27	695
M3	8.83	742
N1	7.67	649
N2	6.83	580
N3	7.56	638
N4	8.62	728
C2	8.16	690
H2	7.65	646
A2	8.18	691

TABLE 8: THICKNESS PROFILE FROM N1 TO N4

STATION (km)	TWO-WAY TRAVEL TIME (μs)	THICKNESS (m)
0	7.68	649
1.0	7.63	645
2.0	7.71	651
3.0	7.74	654
4.0	7.79	658
5.0	7.84	662
6.0	7.90	668
7.0	7.92	669
8.0	7.98	674
9.0	8.02	678
10.0	8.01	677
11.0	8.10	684
12.0	8.19	692
13.0	8.19	692
14.0	8.22	695
15.0	8.26	698
16.0	8.27	699
17.0	8.34	705
18.0	8.39	709
19.0	8.44	713
20.0	8.51	719
21.0	8.56	723
22.0	8.60	727
23.0	8.61	728
24.0	8.61	728
25.0	8.60	727
26.0	8.60	727
27.73	8.65	731
28.64	8.64	730
29.19	8.64	730
29.92	8.66	732
30.69	8.66	732
31.39	8.66	732
32.10	8.68	733
32.74	8.68	733
33.47	8.70	735
34.25	8.66	733
34.99	8.66	733
35.69	8.68	733
36.46	8.66	733
37.26	8.65	731
37.99	8.63	729
38.74	8.63	729
39.45	8.66	733
39.79	8.69	734

TABLE 9: THICKNESS PROFILE FROM A2(CIR) TOWARD N1

STATION (km)	TWO-WAY TRAVEL TIME (μs)	THICKNESS (m)
0.0	8.21	694
0.5	8.28	700
1.0	8.29	701
1.5	8.31	702
2.0	8.31	703
2.5	8.27	699
3.0	8.26	698
3.5	8.25	697
4.0	8.28	699
4.5	8.28	699
5.0	8.27	699
5.7	8.30	701
6.2	8.28	699
6.7	8.25	697
7.2	8.22	694
7.7	8.27	699
8.2	8.26	698
8.7	8.20	693
9.2	8.22	694
9.7	8.24	696
10.0	8.23	696

TABLE 10: THICKNESS PROFILE FROM A2(CIR) TOWARD H2(CIR)

STATION (km)	TWO-WAY TRAVEL TIME (μs)	THICKNESS (m)
0.0	8.24	696
0.5	8.31	702
1.0	8.32	703
1.5	8.27	698
2.0	8.24	696
2.5	8.26	698
3.0	8.23	695
3.5	8.20	692
4.0	8.19	692
4.5	8.18	691
5.0	8.20	692
5.5	8.17	690
6.0	8.25	697
6.5	8.18	690
7.0	8.16	690
7.5	8.15	689
8.0	8.11	685

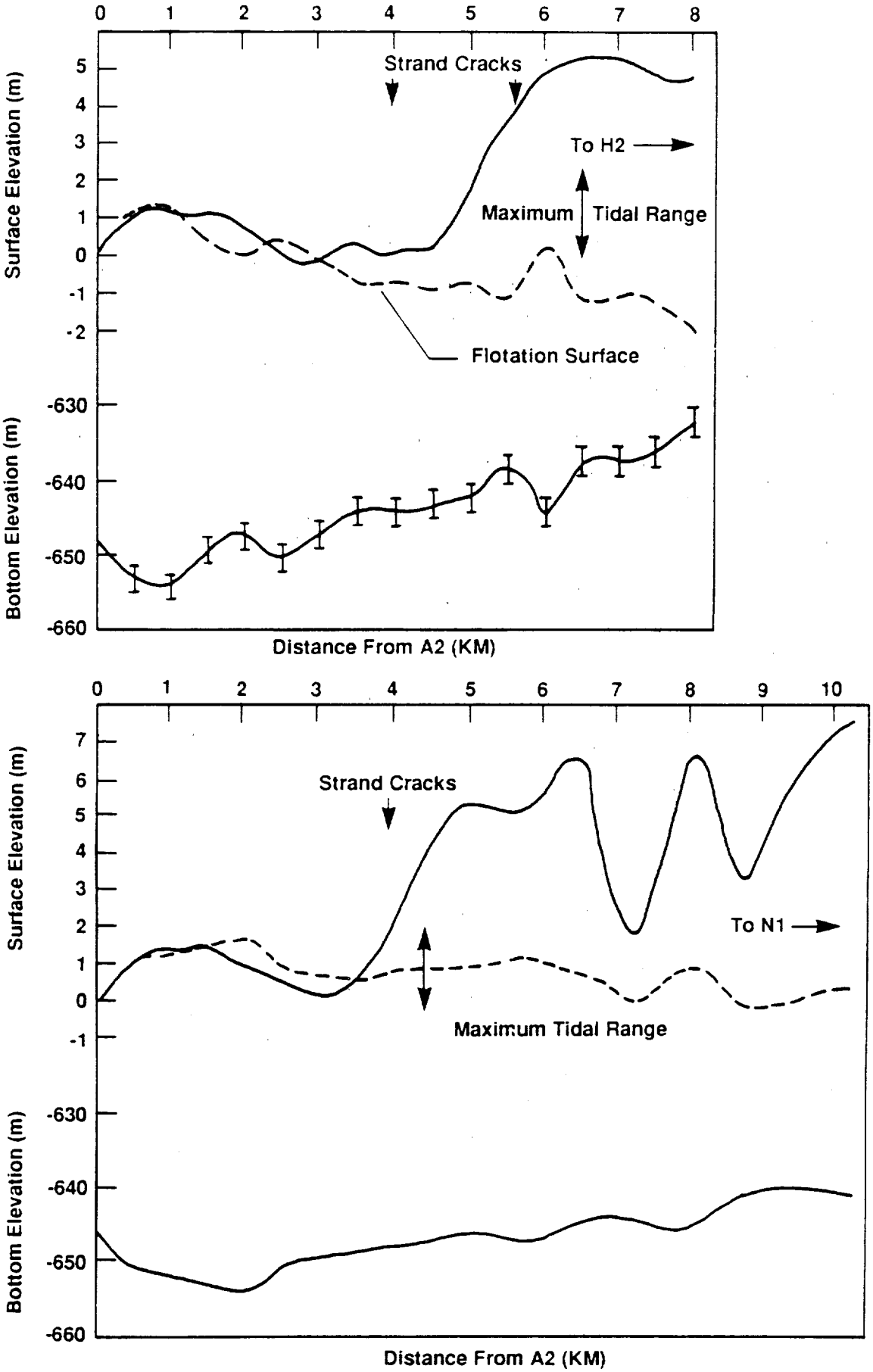

Figure 7: Base and surface topography along two lines near Crary station A2.

SECTION 5: ACCUMULATION RATE

Two methods were used to measure the accumulation rate. The preferred method involved coring to a depth of about 10 m and sampling the core for beta particle activity. There are peaks in this measurement in the 1956 and 1965 horizons associated with global nuclear bomb tests. Cores have been taken at four sites, (DNB, CIR, E19 and DNC) but the analysis has not been completed.

The second method is to repeat measurements of the length of exposed survey stakes. The normal time interval between measurements of stake heights was only 1 year, so the measurement of accumulation rate may not be representative of the longer term average. To convert these stake exposure measurements to mass equivalents, we suggest a value of 388 kg/m^{-3} as the average density of the surface firn.

Table 11 includes these measurements indicating location and the time interval. The standard deviation of the accumulation rate is derived from the eight stake exposures (four survey poles and four adjacent bamboo poles) measured at each strain rosette covering an area of typically 7 km^2. The stake lines at Downstream B usually consist of 10 stakes along an 15-km line.

TABLE 11: ACCUMULATION RATES FROM STAKE EXPOSURES AT STRAIN ROSETTES

STATION	FIRN ACCUM (cm/a)	ICE* EQUIV (cm/a)	DATE
Crary			
A1	50 ± 11	21 ± 5	83,84
A2	58 13	24 6	83,84
	24 7	10 3	84,85
B1	50 6	21 2	83,84
B2	70 11	30 5	83,84
C1	70 4	30 2	83,84
C2	68 12	29 5	83,84
	29 8	12 3	84,85
C3	41 12	17 5	84,85
C4	42 11	18 5	84,85
D1	62 14	26 6	83,84
D2	65 4	28 2	83,84
E'1	20 3	8 1	84,85
E'2	20 12	8 5	84,85
E1	62 3	26 1	84,85
E2	53 11	22 5	84,85
E2.3	19 2	8 1	84,85
E2.5	24 5	10 2	84,85
E3	30 13	13 6	84,85
E4	31 17	13 7	84,85
F1	53 18	22 8	83,84
F2	60 15	25 6	83,84
G1	51 12	22 5	83,84
G2	49 9	21 4	83,84
G3	16 5	7 2	84,85
G4	16 14	7 6	84,85
H1	54 5	23 2	83,84
H2	48 1	20 1	83,84
J1	32 28	14 12	84,85
J2	29 2	12 1	84,85
J3	31 5	13 2	84,85
K1	21 8	9 3	84,85
K2	20 6	8 2	84,85
K3	7 4	3 2	84,85
L1	30 12	13 5	84,85
O	20 5	8 2	84,85
Downstream B			
A11	45 3	19 1	83,84
B25	11 3	5 1	84,85
G1	15 7	6 3	84,85
G2	13 5	6 2	84,85
M0	22 2	9 1	84,85
M1	27 9	11 4	84,85
M2	26 3	11 1	84,85
M3	24 9	10 4	84,85
M4	29 11	12 5	84,85
M5	19 3	8 1	84,85
M6	23 6	10 2	84,85

STATION	FIRN ACCUM (cm/a)	ICE* EQUIV (cm/a)	DATE
Downstream B (cont)			
O	38 ± 5	16 ± 2	83,84
	15 2	6 1	84,85
Downstream C			
A1	26 4	11 2	83,84
A2	27 4	11 2	83,84
B2	16 3	7 1	83,84
C1	21 4	9 2	83,84
C2	18 5	8 2	83,84
O	19 6	8 2	83,84
STAKE LINES			
Downstream B			
C line	46 7	20 3	83,84
D line	44 7	19 3	83,84
E line	46 6	20 2	83,84
F line	44 5	19 2	83,84
A line	48 8	20 3	83,84
Downstream C			
E Line	27 6	11 2	83,84

*Density of firn= 388 kg m^{-3}

SECTION 6: TEN-METER TEMPERATURE AND FIRN DENSITY PROFILES

At the locations where 10-meter-long cores were removed, temperature measurements were made in the resulting holes. In 1983, a single thermistor was used at a single depth, while in 1984 and 1985 a thermistor chain was hung in the hole to measure the vertical temperature gradient. The single thermistors were glass bead Fenwall GB32M2 (2000-ohm resistance at 25 degrees C). The thermistor chain alternated these with Fenwall GB41P2 thermistors (10,000-ohm resistance at 25 degrees C) every meter for 5 m. Each thermistor was calibrated at zero and three sub-zero temperatures. A precision Wheatston bridge (Leeds and Northrup Model 4289-3) was used. The hole was covered to reduce air circulation. Repeated measurements were made as soon as the core was removed to allow the cooling curve to be determined, giving a more accurate estimate of the equilibrium temperature. Measurements were continued until the cooling rate was less than 0.01 degrees C per hour, which usually occurred after 4 to 6 hours. When possible, a final measurement was made after many hours to confirm the calculated equilibrium temperature. Self-heating of the thermistors caused by the 1-mA current output by the measurement bridge limited the accuracy of these temperature measurements to $\pm$ 0.05 degrees C. Table 12 presents these data.

Firn density profiles were calculated using volume and weight data collected at sites where 10-meter-long cores were extracted (Figure 8 and Table 13). In the process of preparing the 10-meter core for shipment, each core was cut into 10-cm sections and weighed to the nearest tenth of a gram using a sheltered triple-beam balance. During the 1983 and 1984 field seasons the weighing was done after each 10-cm section had been placed in a small plastic bag, while in 1985 the core sections were weighed beforehand. The weight of the bags is considered negligible and within the error of these measurements; hence no attempt is made here to adjust the 1983 and 1984 data. In 1983 and 1984 the diameter of the core was taken to be that of the inside diameter of the coring assembly (7.3 cm), while in the 1985 season, each

core section was measured individually using a caliper. The 1985 data showed that the core's diameter varied from the inside diameter of the coring assembly by less than 2mm. Density values obtained from the 10-cm segments of core are assigned to the vertical position of the center point of each segment.

TABLE 12: TEMPERATURE MEASUREMENTS

Station	Date M/D/Y	Depth (m)	Temperature (C)
CIR	12 6 83	10.2	-25.7
	12 2 84	4.0	-26.1
		5.0	-25.5
		6.0	-25.8
		7.0	-25.2
		8.0	-25.1
		9.0	-25.1
		10.0	-25.4
	12 3 84	0.0	-12.0
		1.0	-19.2
		2.0	-24.3
		3.0	-26.0
		4.0	-25.8
		5.0	-26.7
		6.0	-26.7
DNB	11 17 83	9.5	-26.2
	11 19 83	9.5	-26.2
	12 15 84	3.7	-25.9
		4.7	-25.7
		5.7	-26.3
		6.7	-25.2
		7.7	-25.5
		8.7	-25.6
		9.7	-26.1
E19	12 24 85	8.0	-25.9
		9.0	-25.3
		10.0	-26.2
DNC	12 14 83	9.6	-29.8

TABLE 13 (a): FIRN DENSITY PROFILES

DNB CAMP
DEC 1984

DEPTH (m)	DENSITY (gm cm^{-3})	DEPTH (m)	DENSITY (gm cm^{-3})
0.23	.466	5.00	.402
0.33	.411	5.10	.460
0.42	.415	5.20	.434
0.50	.414	5.30	.484
0.57	.421	5.40	.452
0.63	.456	5.49	.437
0.69	.288	5.59	.450
0.76	.383	5.69	.504
0.85	.434	5.79	.488
0.95	.378	5.89	.448
1.05	.402	5.99	.429
1.14	.398	6.09	.442
1.24	.322	6.19	.473
1.34	.406	6.29	.441
1.44	.392	6.39	.463
1.52	.373	6.49	.432
1.61	.392	6.59	.447
1.71	.392	6.69	.482
1.81	.368	6.79	.467
1.90	.358	6.89	.470
1.99	.437	7.00	.465
2.09	.427	7.10	.469
2.18	.388	7.20	.484
2.28	.361	7.30	.461
2.38	.406	7.40	.490
2.48	.324	7.50	.457
2.56	.389	7.60	.502
2.66	.395	7.70	.464
2.75	.478	7.79	.517
2.84	.423	7.89	.504
2.94	.378	7.99	.520
3.32	.460	8.09	.509
3.41	.433	8.19	.488
3.51	.453	8.29	.537
3.60	.375	8.39	.541
3.70	.361	8.49	.472
3.80	.388	8.59	.487
3.90	.420	8.69	.489
4.00	.411	8.78	.483
4.10	.478	8.88	.485
4.20	.366	8.98	.482
4.30	.431	9.08	.507
4.40	.401	9.18	.484
4.50	.437	9.28	.487
4.60	.452	9.39	.509
4.70	.436	9.49	.508
4.80	.407	9.59	.504
4.90	.400		

TABLE 13(b): FIRN DENSITY PROFILES

E19 (DNB)
DEC 1985

DEPTH (m)	DENSITY (gm cm^{-3})	DEPTH (m)	DENSITY (gm cm^{-3})
1.77	.382	6.34	.412
1.87	.374	6.44	.428
1.97	.324	6.54	.426
2.07	.345	6.64	.398
2.17	.312	6.74	.376
2.27	.365	6.84	.345
2.36	.365	6.94	.412
2.45	.341	7.04	.450
2.55	.351	7.14	.433
2.65	.375	7.24	.428
2.75	.358	7.34	.428
2.85	.368	7.44	.436
2.95	.330	7.54	.420
3.05	.427	7.64	.503
3.15	.284	7.73	.424
3.25	.312	7.83	.430
3.35	.400	7.93	.438
3.45	.352	8.03	.481
3.55	.364	8.13	.432
3.65	.357	8.23	.466
3.75	.394	8.33	.489
3.85	.411	8.43	.474
3.95	.388	8.53	.450
4.05	.313	8.63	.487
4.15	.376	8.73	.520
4.25	.388	8.83	.408
4.35	.379	8.93	.515
4.45	.363	9.03	.453
4.55	.393	9.13	.457
4.65	.365	9.23	.491
4.75	.357	9.33	.518
4.85	.388	9.43	.529
4.95	.403	9.53	.497
5.05	.396	9.63	.496
5.15	.374	9.73	.529
5.25	.442	9.83	.483
5.35	.347	9.93	.496
5.45	.434	10.03	.492
5.55	.387	10.13	.514
5.64	.406	10.23	.518
5.74	.408	10.33	.472
5.84	.430	10.43	.520
5.94	.388	10.53	.528
6.04	.396	10.63	.530
6.14	.419	10.73	.508
6.24	.437	10.81	.549

TABLE 13(c): FIRN DENSITY PROFILES

CIR CAMP
DEC 1984

DEPTH (m)	DENSITY (gm cm^{-3})	DEPTH (m)	DENSITY (gm cm^{-3})
0.05	.396	5.05	.431
0.15	.345	5.15	.368
0.25	.366	5.25	.392
0.35	.323	5.35	.433
0.45	.330	5.45	.427
0.55	.411	5.55	.392
0.65	.369	5.65	.353
0.75	.357	5.75	.425
0.85	.306	5.85	.460
0.95	.290	5.95	.477
1.05	.278	6.05	.467
1.15	.464	6.15	.456
1.25	.314	6.25	.415
1.35	.386	6.35	.424
1.45	.382	6.45	.470
1.55	.352	6.55	.479
1.65	.337	6.65	.440
1.75	.384	6.75	.445
1.85	.274	6.85	.428
1.95	.409	6.95	.390
2.05	.331	7.05	.462
2.15	.383	7.15	.482
2.25	.318	7.25	.458
2.35	.355	7.35	.461
2.45	.371	7.45	.421
2.55	.409	7.55	.459
2.65	.334	7.65	.477
2.85	.459	7.75	.477
2.95	.349	7.85	.499
3.05	.395	7.95	.486
3.15	.324	8.05	.534
3.25	.282	8.15	.525
3.35	.354	8.25	.504
3.45	.302	8.35	.504
3.55	.384	8.45	.486
3.65	.374	8.55	.452
3.75	.390	8.65	.517
3.85	.381	8.75	.525
3.95	.318	8.85	.539
4.05	.394	8.95	.489
4.15	.458	9.05	.525
4.25	.412	9.15	.522
4.35	.355	9.25	.507
4.45	.401	9.35	.491
4.55	.383	9.45	.540
4.65	.348	9.55	.527
4.75	.352	9.65	.515
4.85	.400	9.75	.494
4.95	.423	9.85	.510
		9.95	.549

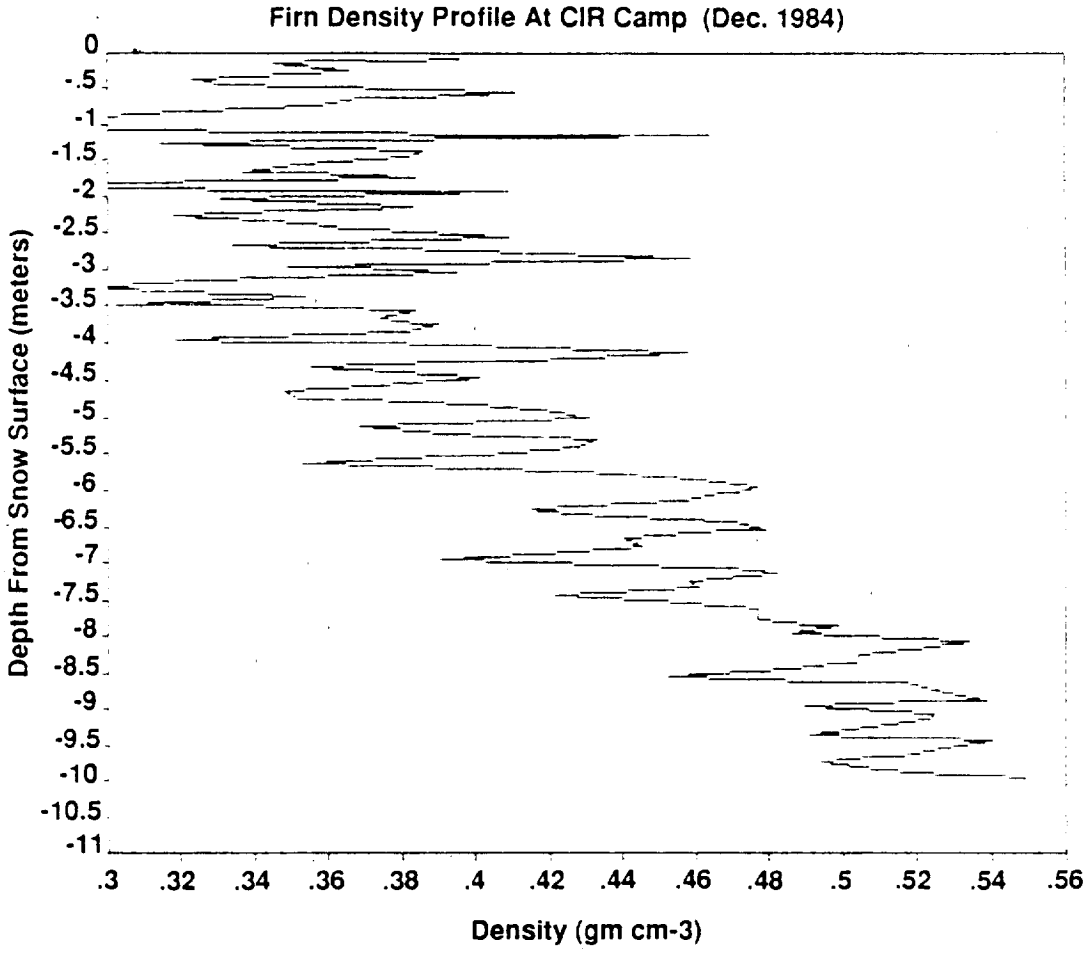

Figure 8 (a-c): Firn density profiles.

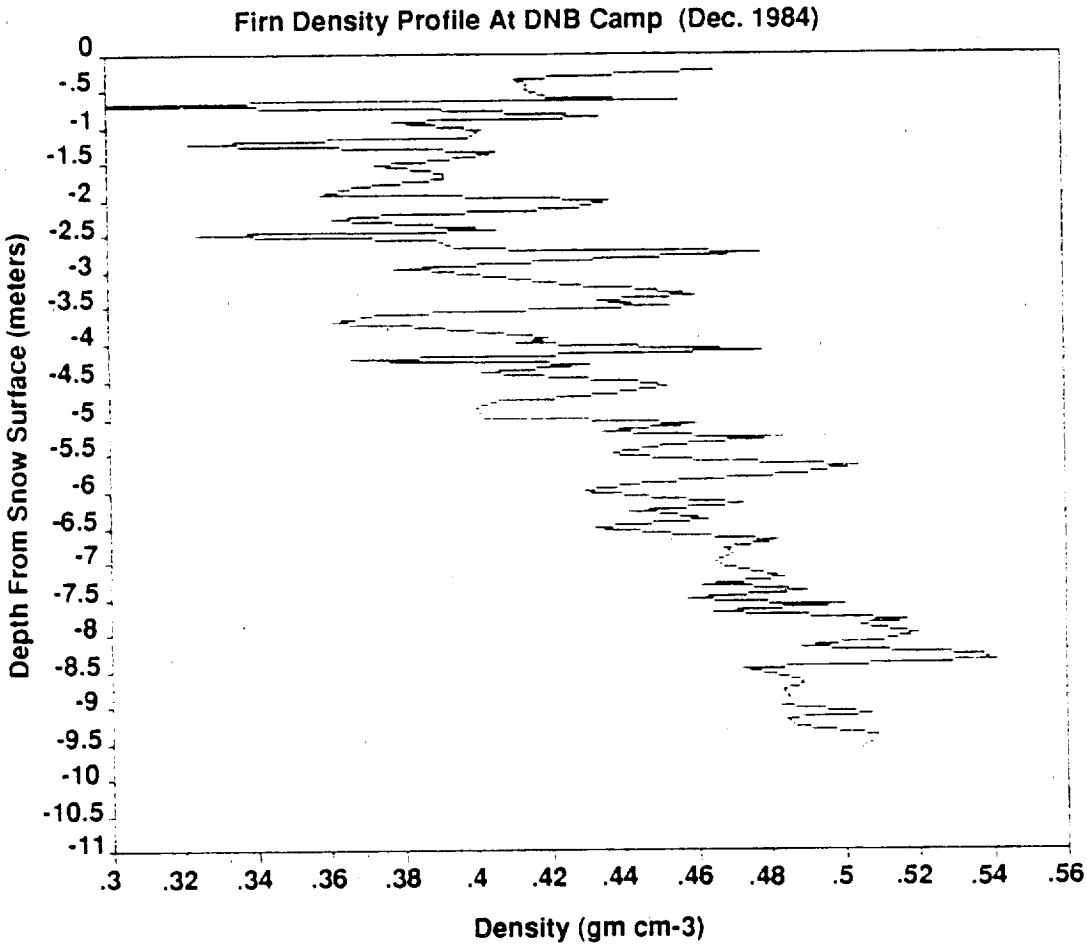
Firn Density Profile At DNB Camp (Dec. 1984)
Depth From Snow Surface (meters)
0
-.5
-1
-1.5
-2
-2.5
-3
-3.5
-4
-4.5
-5
-5.5
-6
-6.5
-7
-7.5
-8
-8.5
-9
-9.5
-10
-10.5
-11
.3
.32
.34
.36
.38
.4
.42
.44
.46
.48
.5
.52
.54
.56
Density (gm cm-3)

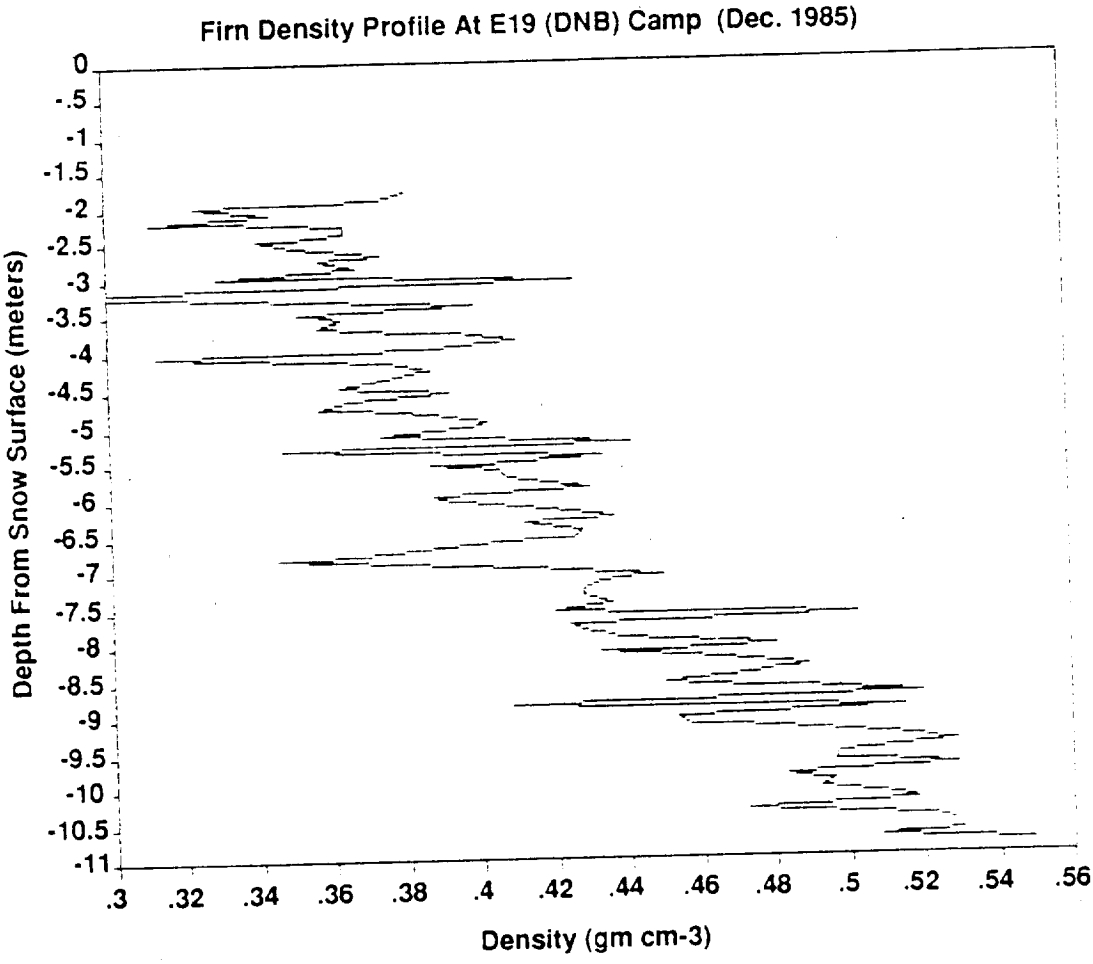
Firn Density Profile At E19 (DNB) Camp (Dec. 1985)
Depth From Snow Surface (meters)
0
-.5
-1
-1.5
-2
-2.5
-3
-3.5
-4
-4.5
-5
-5.5
-6
-6.5
-7
-7.5
-8
-8.5
-9
-9.5
-10
-10.5
-11
.3
.32
.34
.36
.38
.4
.42
.44
.46
.48
.5
.52
.54
.56
Density (gm cm-3)

SECTION 7: SPECIAL SITES
RESULTS FROM DOUBLE STAKE LINES AT L1 AND DNB

Special sites refer to two areas where double stake lines were established to determine the detailed strain field in an extended region. The relative velocities and strain rate were determined as previously described in Section 2

TABLE 14: VELOCITY PROFILE FROM DOUBLE LINE OF STAKES WHICH CROSSES THE EDGE OF CRARY ICE RISE NEAR STATION L1 (see Fig 11(a))

STATION NAME	COORDINATES* X (m)	Y (m)	VELOCITY X-comp. (m/a)	Y-comp. (m/a)
W	50000.00	50000.00	0.00	0.00
X	49590.38	50187.44	0.51	1.06
A3	50468.18	50180.27	0.52	-1.13
Y	49741.70	50964.61	2.75	1.02
A2	50505.86	50981.21	2.73	-0.88
Z	49827.13	51614.92	4.78	1.22
A1	50536.26	51583.82	4.67	-0.63
A0	49860.28	52300.72	9.66	1.46
0	50572.51	52265.96	8.56	-0.41
A	49879.28	52737.89	22.90	2.33
1	50782.65	52820.14	23.85	-0.02
B	49886.65	53322.97	42.55	3.56
2	50752.39	53544.42	48.81	1.67
C	49914.35	54282.94	74.44	5.04
3	50747.48	54509.57	81.04	2.21
D	49954.55	55430.03	109.08	5.00
4	50852.28	55476.13	110.58	2.31
E	49991.85	56612.34	141.96	4.56
5	50989.94	56690.43	144.82	1.13
F	50027.91	57774.16	173.96	3.52
6	51043.10	57828.09	176.34	0.46
G	50062.47	58725.45	197.69	2.64
7	51085.83	58867.63	202.36	-0.56
H	50093.00	59677.40	219.57	1.96
8	51135.38	59928.41	226.66	-1.83
I	50125.66	60685.17	241.91	1.02
9	51175.01	60694.78	243.77	-2.77
J	50190.23	61808.99	265.53	-0.33
10	51231.68	61743.33	265.92	-4.23

*Azimuth of X-axis is 316.9 degrees. Geographic coordinates of station W are: S83°06'11", W172° 25'23".

TABLE 15: STRAIN RATE PROFILE FROM DOUBLE LINE OF STAKES WHICH CROSSES THE EDGE OF CRARY ICE RISE AT STATION L1 (see Fig. 9)

STATIONS	COORDINATES* X(m)	Y(m)	P1+ ($10^{-3}a^{-1}$)	P2+ ($10^{-3}a^{-1}$)	P3+ ($10^{-3}a^{-1}$)	ANGLE OF P1 WRT X-axis*
W X A3	50019	50122	0.2± 0.2	-0.0 ±0.2	-0.2± 0.3	59.3 ± 0.3
X A3 Y	49933	50444	0.52 0.06	-0.04 0.09	-0.5 0.1	67.74 0.08
A3 Y A2	50238	50708	0.45 0.06	-0.12 0.09	-0.3 0.1	76.70 0.08
Y A2 Z	50025	51187	0.75 0.07	-0.2 0.1	-0.5 0.1	69.65 0.05
A2 Z A1	50290	51393	0.69 0.08	-0.1 0.1	-0.5 0.1	65.18 0.07
Z A1 A0	50074	51833	2.59 0.08	-1.95 0.08	-0.6 0.1	46.99 0.01
A1 A0 0	50323	52050	1.39 0.09	-2.21 0.08	0.8 0.1	59.48 0.01
A0 0 A	50104	52434	14.9 0.1	-12.9 0.1	-2.0 0.1	47.24 0.00
0 A 1	50411	52608	12.92 0.08	-12.69 0.08	-0.2 0.1	48.65 0.00
A 1 B	50182	52960	15.61 0.08	-15.49 0.08	-0.1 0.1	48.83 0.00
1 B 2	50473	53229	16.26 0.07	-15.60 0.07	-0.65 0.09	48.41 0.00
B 2 C	50184	53716	15.57 0.06	-15.23 0.06	-0.34 0.08	47.70 0.00
2 C 3	50471	54112	14.63 0.06	-15.26 0.06	0.63 0.08	46.64 0.00
C 3 D	50205	54704	13.30 0.06	-13.50 0.05	0.21 0.08	45.42 0.00
3 D 4	50518	55138	14.04 0.06	-13.50 0.06	-0.54 0.08	45.35 0.00
D 4 E	50266	55839	12.39 0.05	-12.43 0.05	0.04 0.08	44.40 0.00
4 E 5	50611	56259	12.42 0.05	-12.34 0.05	-0.07 0.07	43.56 0.00
E 5 F	50336	57025	12.05 0.05	-12.14 0.05	0.86 0.07	43.23 0.00
5 F 6	50687	57430	12.57 0.05	-12.14 0.05	-0.43 0.07	43.45 0.00
F 6 G	50377	58109	11.12 0.05	-10.90 0.06	-0.21 0.08	42.60 0.00
6 G 7	50730	58474	11.14 0.05	-10.91 0.05	-0.22 0.07	42.46 0.00
G 7 H	50413	59090	10.37 0.06	-9.62 0.06	-0.76 0.08	42.15 0.00
7 H 8	50771	59491	9.92 0.05	-9.67 0.05	-0.25 0.07	41.59 0.00
H 8 I	50451	60097	9.72 0.05	-9.09 0.05	-0.64 0.08	41.50 0.00
8 I 9	50812	60436	9.68 0.06	-9.15 0.07	-0.53 0.09	41.03 0.00
I 9 J	50497	61063	9.05 0.06	-8.47 0.07	-0.58 0.07	40.78 0.00
9 J 10	50865	61416	8.98 0.07	-8.47 0.06	-0.50 0.08	40.23 0.00

*Azimuth of X-axis is 316.9 degrees

+P1 and P2 are principal axes of horizontal tension and compression, respectively. P3= -(P1+P2) is vertical strain rate

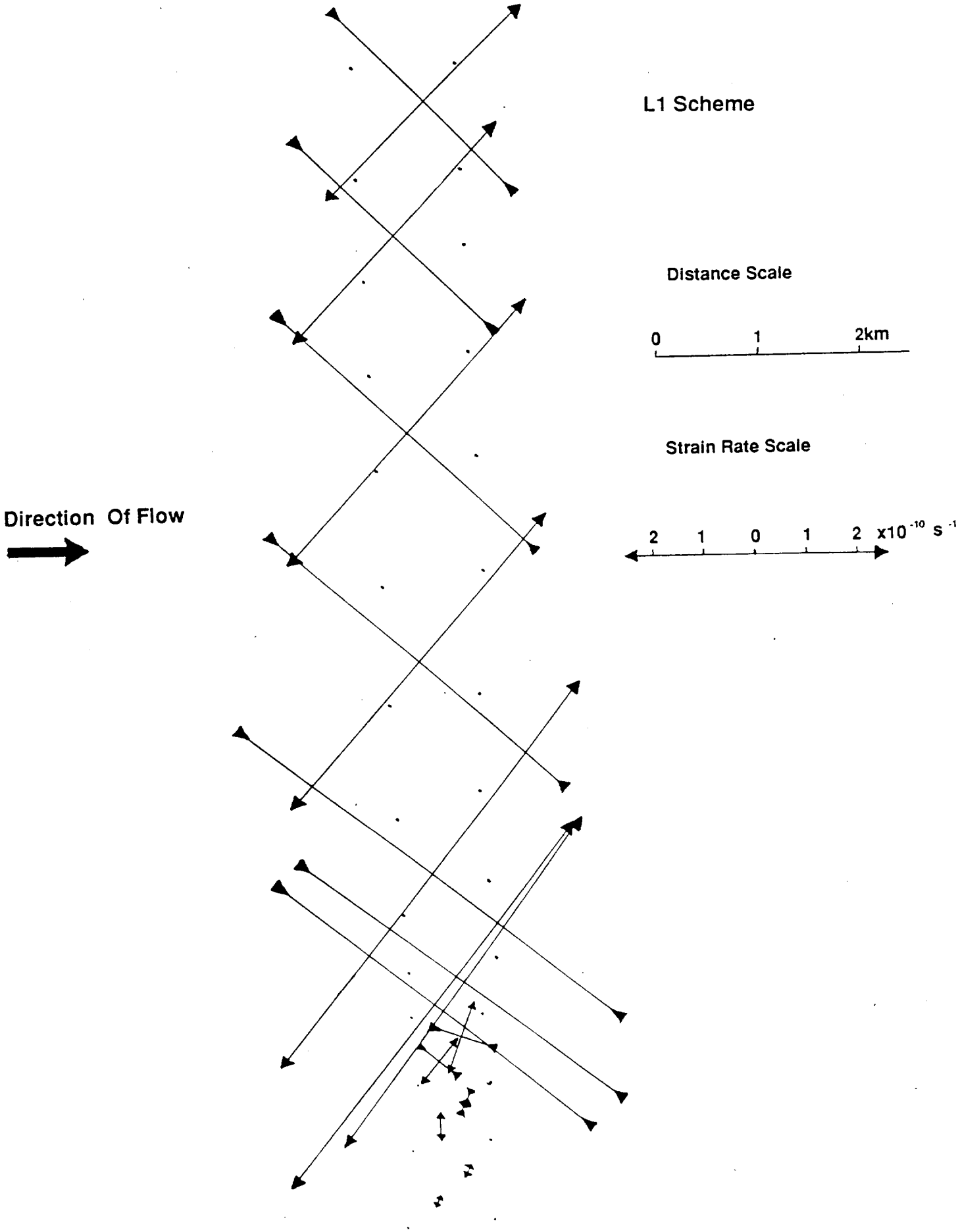

Figure 9: Strain rates measured along a double stake line at L1, across the margin of Crary Ice Rise.

TABLE 16: VELOCITY PROFILE FROM DOUBLE LINE OF STAKES PARALLEL TO FLOW IN THE MOUTH OF ICE STREAM B.

STATION NAME	COORDINATES* X (m)	Y (m)	VELOCITY X-comp. (m/a)	Y-comp. (m/a)
F10	48722.25	65058.83	-47.29	495.84
E10	47123.69	64442.66	-53.71	498.97
F9	48667.88	63612.12	-51.58	497.55
E9	47083.31	63002.17	-57.15	500.27
F8	48614.64	62199.78	-55.19	498.63
E8	47043.61	61580.14	-60.07	501.56
F7	48559.75	60746.05	-58.74	499.84
E7	47004.03	60149.06	-63.26	502.21
F6	48504.94	59312.11	-61.99	501.06
E6	46965.05	58715.93	-65.90	502.75
F5	48450.11	57894.97	-64.67	502.02
E5	46925.04	57248.23	-68.72	503.54
F4	48394.46	56468.13	-67.50	502.78
E4	46885.73	55817.89	-70.98	504.50
F3	48338.80	55037.41	-70.06	504.54
E3	46845.75	54354.00	-74.02	505.78
F2	48283.48	53615.69	-73.13	506.66
E2	46804.46	52842.80	-78.67	507.22
F1	48238.29	52169.61	-77.17	508.23
E1	46765.76	51429.91	-83.15	508.76
A1	48660.00	50000.00	-83.96	510.92
A2	47208.94	50000.00	-86.21	510.74
D1	48138.31	49481.45	-86.68	511.58
C1	46786.96	48832.68	-91.37	511.56
D2	48091.78	48221.00	-91.18	512.99
C2	46861.04	47383.77	-96.03	513.81
D3	48040.47	46856.76	-95.49	514.64
C3	46936.43	45934.86	-100.61	515.35
D4	47991.46	45543.27	-99.90	516.02
C4	47013.62	44481.85	-104.74	516.90
D5	47942.21	44218.70	-104.21	517.35
C5	47090.69	43038.58	-108.88	518.34
D6	47892.79	42887.81	-108.17	518.78
C6	47169.13	41569.26	-113.30	519.28
D7	47843.64	41564.22	-112.25	519.62
C7	47243.96	40177.83	-118.18	520.49
D8	47778.92	39804.28	-118.64	521.08
C8	47318.40	38791.39	-121.23	521.17
D9	47730.55	38479.92	-121.70	521.77
C9	47396.86	37328.70	-125.18	522.68
D10	47683.85	37153.12	-125.62	523.23
C10	47471.54	35941.58	-128.17	523.51

*Azimuth of X-axis is 289.7 degrees. Geographic coordinates of station A1 are: S84° 10'52", W154° 10'08".

TABLE 17: STRAIN RATE PROFILE FROM DOUBLE LINE OF STAKES WHICH PARALLELS ICE FLOW IN THE MOUTH OF ICE STREAM B (see Fig. 10)

STATIONS			COORDINATES* X(m)	Y(m)	P1 ($10^{-3}a^{-1}$)	P2 ($10^{-3}a^{-1}$)	P3 ($10^{-3}a^{-1}$)	ANGLE OF P1 WRT X-axis*
F10	E10	F9	48171	64371	3.02±0.01	-1.24±0.04	-1.79±0.05	9.14±0.00
E10	F9	E9	47625	63686	2.68 0.01	-.93 0.05	-1.76 0.05	7.49 0.00
F9	E9	F8	48122	62938	2.65 0.01	-.79 0.05	-1.86 0.05	8.61 0.00
E9	F8	E8	47580	62261	2.34 0.01	-.88 0.05	-1.46 0.05	4.15 0.00
F8	E8	F7	48073	61509	2.23 0.01	-.82 0.05	-1.41 0.05	7.59 0.01
E8	F7	E7	47536	60825	2.14 0.01	-.48 0.05	-1.66 0.05	9.01 0.01
F7	E7	F6	48023	60069	2.15 0.01	-.89 0.05	-1.26 0.05	9.31 0.01
E7	F6	E6	47491	59392	1.92 0.01	-.43 0.05	-1.49 0.05	10.27 0.01
F6	E6	F5	47973	58641	1.93 0.02	-.73 0.05	-1.20 0.05	10.71 0.01
E6	F5	E5	47447	57953	1.98 0.02	-.64 0.05	-1.35 0.05	12.32 0.01
F5	E5	F4	47923	57204	1.98 0.02	-.63 0.05	-1.35 0.05	12.73 0.01
E5	F4	E4	47402	56511	1.70 0.01	-.69 0.05	-1.00 0.05	8.07 0.01
F4	E4	F3	47873	55774	1.67 0.02	-1.32 0.04	-.35 0.05	10.92 0.01
E4	F3	E3	47357	55070	1.95 0.02	-1.09 0.04	-.86 0.05	15.88 0.01
F3	E3	F2	47823	54336	1.97 0.02	-1.75 0.04	-.22 0.05	15.74 0.00
E3	F2	E2	47311	53604	2.82 0.02	-1.60 0.04	-1.22 0.05	22.57 0.00
F2	E2	F1	47775	52876	2.86 0.02	-1.63 0.04	-1.23 0.05	20.22 0.00
E2	F1	E1	47270	52147	3.14 0.02	-1.74 0.04	-1.40 0.05	21.21 0.00
F1	E1	A1	47888	51200	3.11 0.02	-2.04 0.03	-1.08 0.04	23.86 0.00
E1	A1	A2	47545	50477	2.10 0.03	-1.89 0.05	-.21 0.06	21.73 0.01
A1	A2	D1	48002	49827	2.48 0.05	-2.34 0.09	-.15 0.10	26.13 0.01
A2	D1	C1	47378	49438	2.85 0.03	-2.08 0.05	-.77 0.06	29.87 0.01
D1	C1	D2	47672	48845	2.83 0.03	-2.18 0.05	-.64 0.05	27.11 0.00
C1	D2	C2	47247	48146	2.53 0.03	-2.37 0.04	-.16 0.05	24.38 0.00
D2	C2	D3	47664	47487	2.54 0.03	-1.91 0.05	-.63 0.05	23.38 0.00
C2	D3	C3	47279	46725	2.73 0.03	-1.86 0.04	-.87 0.05	24.80 0.00
D3	C3	D4	47656	46112	2.72 0.03	-1.88 0.05	-.84 0.06	25.01 0.00
C3	D4	C4	47314	45320	2.48 0.03	-1.77 0.05	-.71 0.06	24.18 0.01
D4	C4	D5	47649	44748	2.34 0.04	-1.88 0.05	-.46 0.06	26.84 0.01
C4	D5	C5	47349	43913	2.19 0.04	-1.76 0.05	-.42 0.06	26.40 0.01
D5	C5	D6	47642	43382	2.24 0.04	-1.89 0.05	-.35 0.07	26.22 0.01
C5	D6	C6	47384	42498	2.46 0.04	-1.62 0.05	-.84 0.06	29.69 0.01
D6	C6	D7	47635	42007	2.54 0.05	-1.62 0.06	-.92 0.08	28.84 0.01
C6	D7	C7	47419	41104	2.74 0.05	-2.00 0.06	-.74 0.07	29.69 0.01
D7	C7	D8	47622	40515	2.77 0.05	-2.00 0.06	-.78 0.08	29.38 0.01
C7	D8	C8	47447	39591	1.74 0.05	-1.50 0.06	-.25 0.08	34.62 0.01
D8	C8	D9	47609	39025	1.78 0.06	-1.75 0.07	-.03 0.10	35.44 0.01
C8	D9	C9	47482	38200	1.96 0.07	-2.01 0.07	.05 0.10	30.45 0.01
D9	C9	D10	47604	37654	1.77 0.09	-2.65 0.10	.88 0.14	35.70 0.01
C9	D10	C10	47517	36808	1.52 0.10	-2.26 0.10	.74 0.14	42.80 0.01

*Azimuth of X-axis is 289.7 degrees. Geographic coordinates of station A1 are: S84°10'52", W154°10'08".

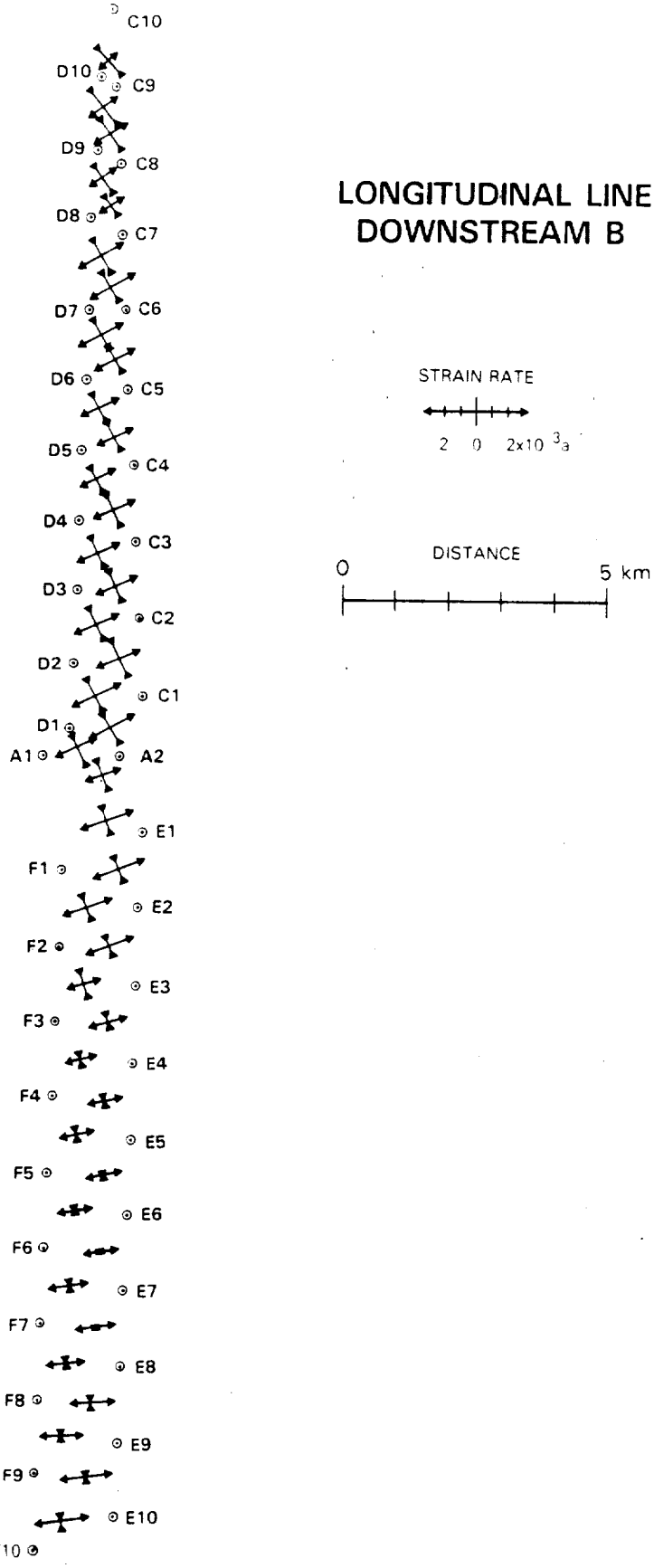

Figure 10: Longitudinal profile of strain rates measured along a double stake line near DNB.

SECTION 8: AERIAL PHOTOGRAPHY

In January 1985 the U. S. Geological Survey took aerial photographs of the Crary Ice Rise. The photographs covered an area of approximately 175 km by 70 km and were taken at an altitude of 25,000 feet. In all, 570 photographs were obtained. Using every other photograph, a mosaic was created by matching features (stratsugi and crevasses) on adjacent photographs. Overlays were then prepared of crevasses, crests of undulations and open rifts in the ice shelf downstream of the ice rise. Identification of ground control stations provided an estimation of the scale to be 1:47,400. The mosaic and overlays were then photographically reduced to scales of 1:250,000 and 1:500,000. Figures 11(a) and 11(b) show the crevasse and undulation overlays with a geographic grid.

There is a gap in the photographic coverage along a thin strip to the grid northeast of the ice rise. Bad weather forced the data to be collected in two missions separated by 3 days. While an extra photographic strip was taken to provide ample overlay, poor navigation caused errors in position large enough to create the gap. Fortunately, there were two control points on the smaller mosaic which allowed a separate calculation of scale, and allowed this piece to be aligned relative to the larger section. The gap is relatively small and its effect on the mapped features is small. The most apparent difference in the two data sets are the crevasses downstream of the ice rise. In the smaller mosaic, more crevasses are apparent compared to the larger mosaic. This is most likely a result of differing solar azimuth and elevation at the time of each photographic mission.

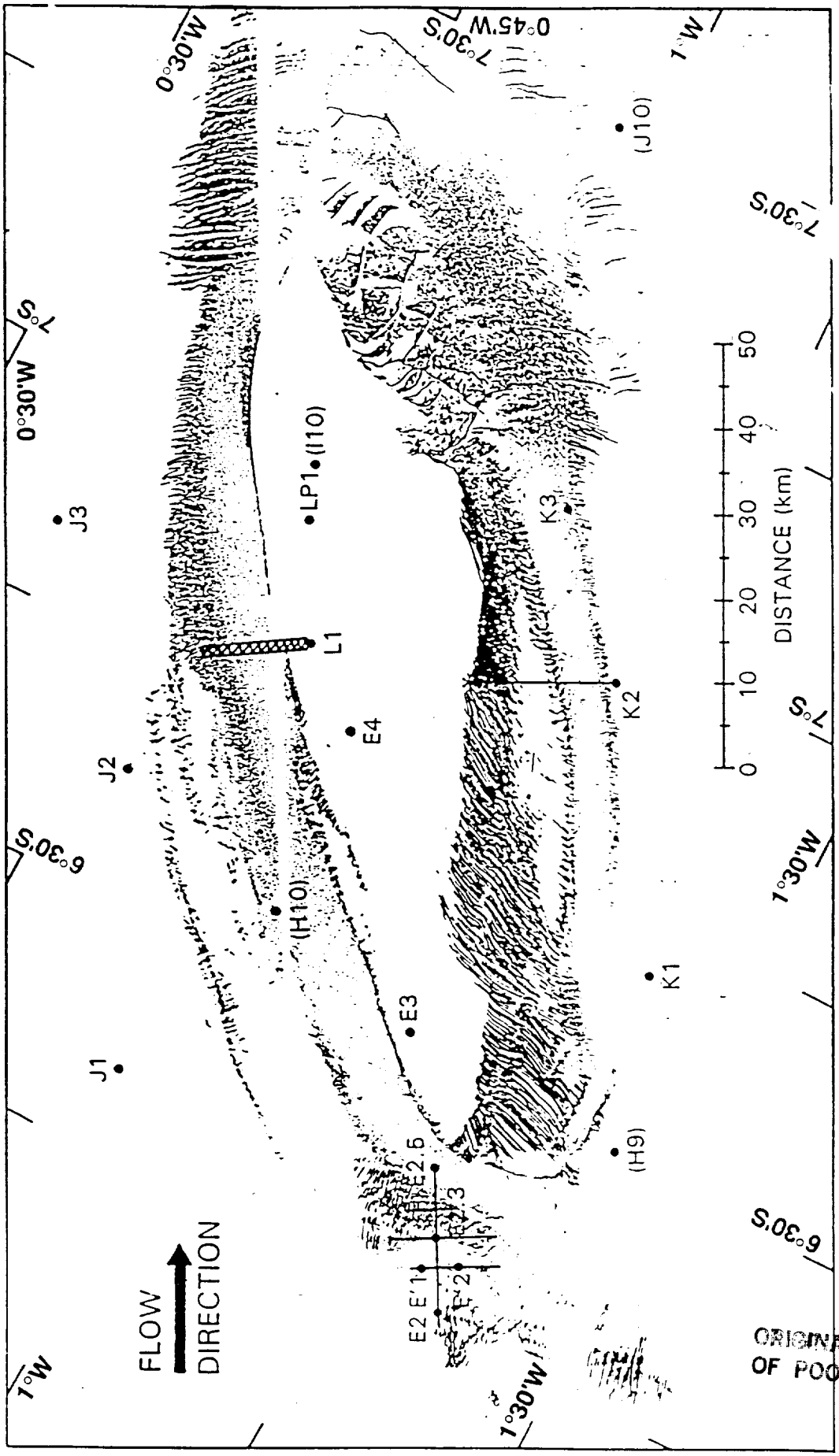

Figure 11 (a-b): Crevasse and undulation traces from aerial photography of Crary Ice Rise.

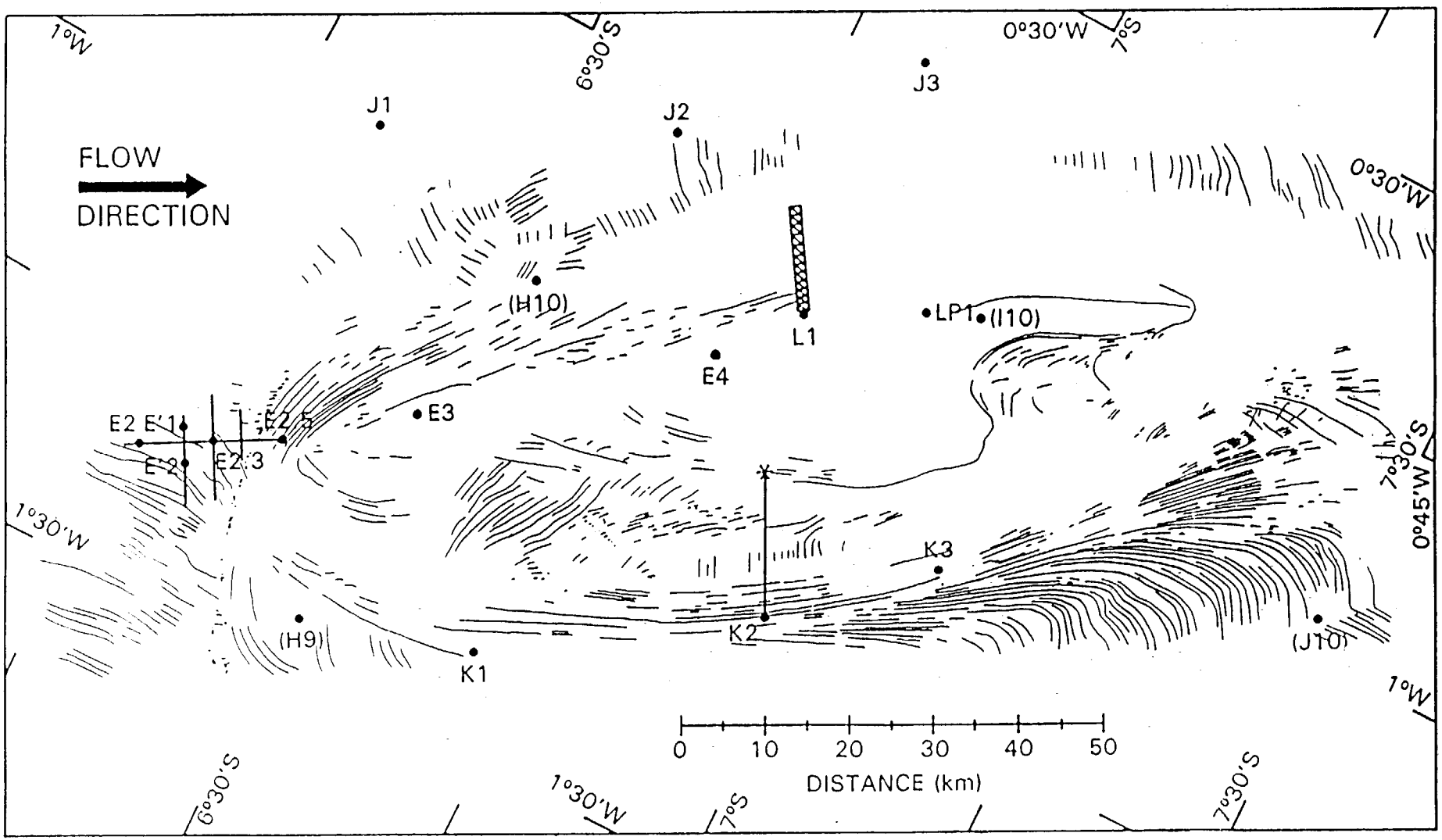
1°W
6°30'S
0°30'W
7°S
J1
J2
J3
FLOW
DIRECTION
(H10)
L1
LP1
(I10)
E4
E3
E2 E'1
E'2
E2 3
E2 5
1°30'W
K3
K2
(H9)
K1
(J10)
0°45'W
7°30'S
0
10
20
30
40
50
DISTANCE (km)

SECTION 9: MULTI-LEG ROSETTES

The multi-leg strain rosette technique outlined in MacAyeal (1985) was used at three stations near the grounding line of the ice stream, N1, N3 and N4. A fourth multi-leg rosette was planted at N2, but it was not resurveyed by the end of the 1985-1986 field season. This technique was chosen because it provides a means of reducing measurement uncertainty under circumstances where the time period between initial station deployment and resurvey is short. Our goal was to recover the strain rate data after approximately 15 days. A redundancy of 40 measurement legs was used by planting 10 outlying stakes and surveying them from four independent central stakes. The details of this innovative method are discussed in Appendix 3. The data are presented in Table 18. Figure 12 shows the similarity of velocities of the ten outlying stakes relative to the velocity of four center stakes. The computed strain rate is indicated in the center of this figure. Figure 13 indicates the scatter of calculated strain rates.

TABLE 18: MULTI-LEG ROSETTE RESULTS

18(a): Comparison between weighted, unweighted and linear method*

	Single Value Decomposition											
	Weighted Method				Unweighted Method				Linear Method			
	P1	P2	PZ	P1-Azimuth d m d	P1	P2	PZ	P1-Azi d m	P1	P2	PZ	P1-Azi d m
C3	0.22±0.03	-0.09±0.02	-0.13±0.04	077-33±4.2	0.17	-0.06	-0.17	080-52	0.20	-0.06	-0.14	079
E'1	13.60 0.03	-13.87 0.03	0.27 0.04	070-42 .05	13.59	13.94	0.35	070-36	13.6	-13.9	0.3	070-36
E'2	16.95 0.03	-13.61 0.03	-3.61 0.04	061-06 .02	16.60	-13.77	-2.83	060-04	16.6	-13.8	-2.8	060-06
E2.3	29.89 0.03	-24.43 0.03	-5.46 0.05	076-25 .01	29.41	-22.18	-7.23	074-08	28.8	-22.8	-6.0	074-13
E2.5	28.08 0.03	-37.33 0.03	9.25 0.04	056-31 .01	30.76	-37.99	7.23	060-27	30.9	-37.9	7.0	060-42
E3	1.52 0.03	-0.20 0.03	1.33 0.04	084-56 .78	1.42	-0.20	-1.21	090-54	1.41	-0.24	-1.17	089-24
E4	0.80 0.02	0.14 0.03	-0.95 0.04	342-31 1.8	0.80	0.27	-1.07	344-46	0.80	0.25	-1.05	344
J1	2.81 0.03	-2.45 0.03	-0.36 0.04	069-11 .24	2.86	-2.40	-0.46	068-36	2.88	-2.35	-0.51	068-30
J2	2.79 0.03	-2.85 0.03	0.06 0.04	096-08 .21	2.83	-2.62	-0.21	094-51	2.83	-2.62	-0.21	094-54
J3	1.67 0.03	0.45 0.03	-2.12 0.05	318-16 1.1	1.67	0.44	-2.11	318-42	1.67	0.46	-2.13	318

18(b): Comparison of 3-leg, 10-leg and 40-leg rosette data from N3+

3-leg rosettes

	P2	P1	PZ	P1-Azimuth d m
A1 E1 H1	-2.08	2.00	0.75	337-34
B1 F1 I1	-1.45	2.04	-0.60	338-13
C1 G1 J1	-1.64	1.66	-0.02	335-32
A2 E2 H2	-2.18	1.97	0.20	337-10
B2 F2 I2	-1.56	2.12	-0.56	342-11
C2 G2 J2	-1.52	1.52	0.00	334-49
A3 E3 H3	-2.17	1.91	0.26	336-46
B3 F3 I3	-1.54	1.91	-0.37	340-27
C3 G3 J3	-1.59	1.50	0.09	334-20
A4 E4 H4	-2.14	1.89	0.25	336-40
B4 F4 I4	-1.72	2.08	-0.36	240-59
C4 G4 J4	-1.90.	2.21	-0.31	335-24
Sample Mean	-1.8±0.3	1.9±0.3	-0.1±0.3	337-30

10-leg rosette

	P2	P1	PZ	P1-Azimuth d m
A1 - J1	-1.69 0.04	1.65 0.03	0.05 0.05	335-51
A2 - J2	-1.68 0.04	1.75 0.03	-0.07 0.05	337-45
A3 - J3	-1.71 0.04	1.65 0.03	-0.06 0.05	334-38
A4 - J4	-1.84 0.04	1.54 0.03	0.30 0.05	335-47
Sample Mean	-1.73±0.07	1.65±0.09	0.07±0.16	336-00

40-leg rosette

	P2	P1	PZ	P1-Azimuth d m
A1 - J40	-1.73±0.02	1.62±0.02	0.11±0.03	335-46

+Strain rates are in units of ($x10^{-10}$ s^{-1})

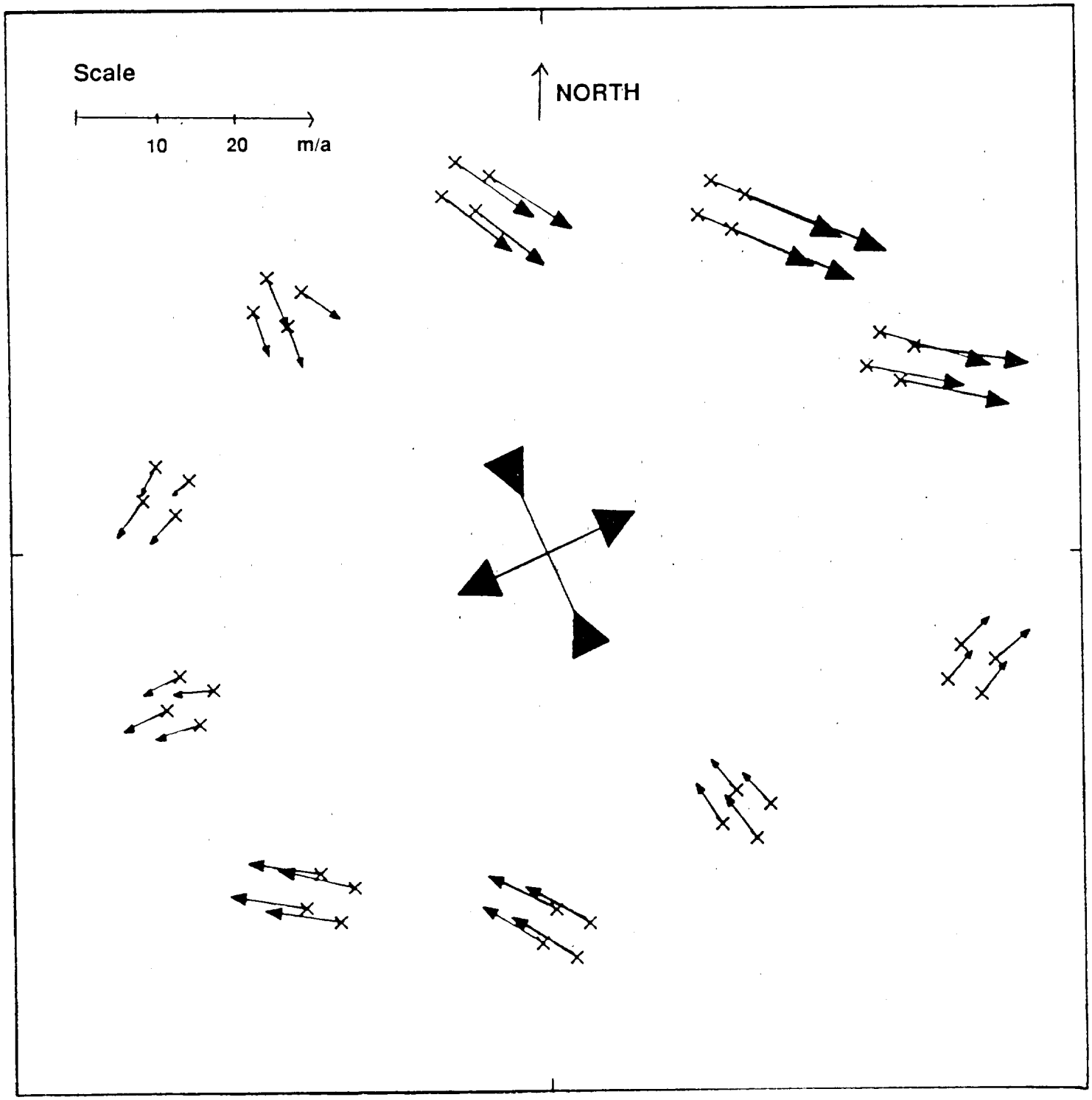

Figure 12-13: Stake movements and strain rates at station N3 from multi-leg rosette results.

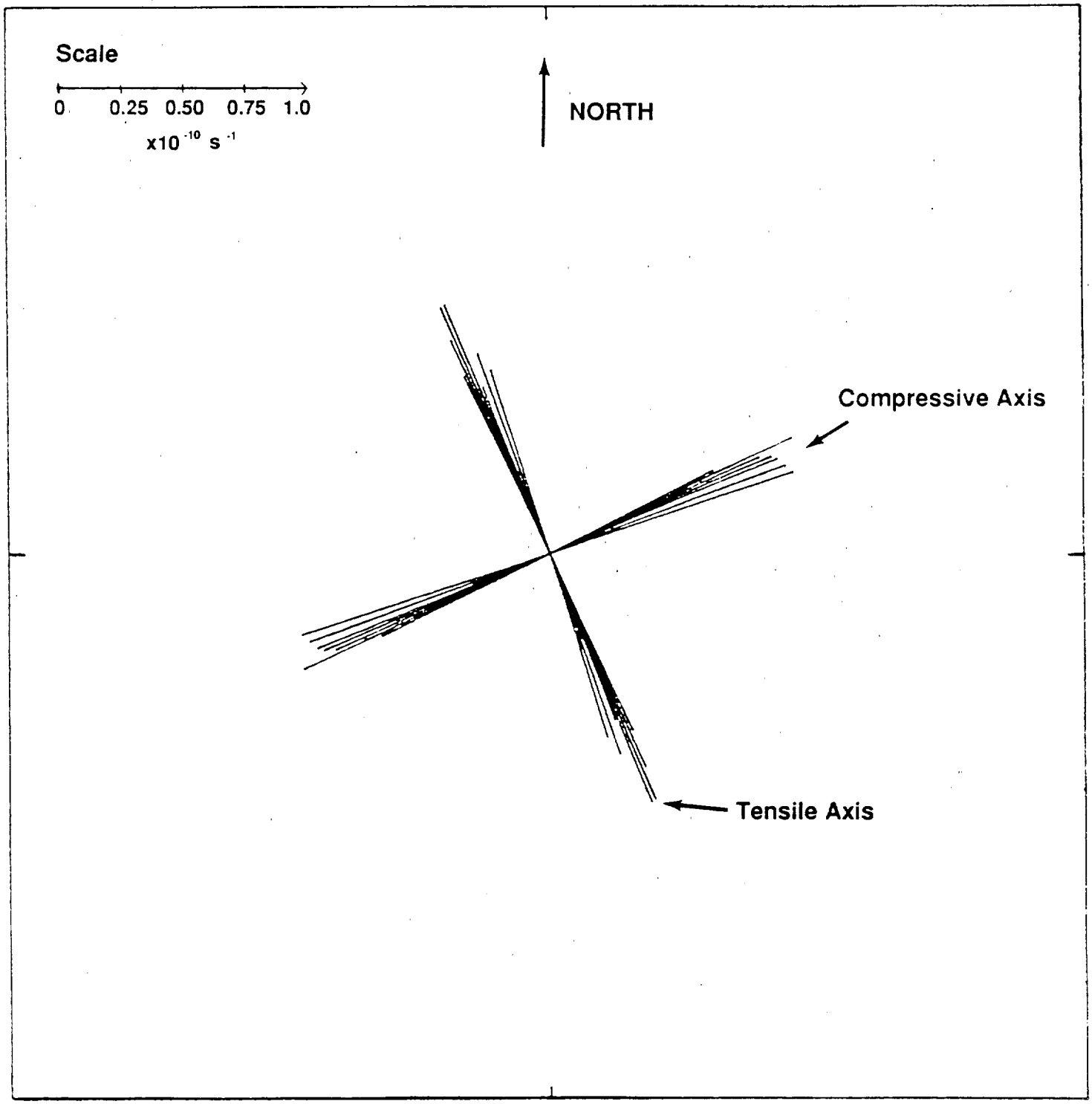
Scale
0 0.25 0.50 0.75 1.0
x10 -10 s -1
NORTH
Compressive Axis
Tensile Axis

ACKNOWLEDGEMENTS

These data were collected due to the considerable efforts of the following field assistants: James Foster, Richard Otto, John Scofield, Matthew Sturm, David Thompson and Jay Zwally. Publications from these data (Appendix 4) will never adequately reflect their sacrifices made to this field program.

This research was supported by NSF grants DPP-8207320, DPP-8405287 and DPP-8514543.

References:

Boas, M. L., 1983. Mathematical Methods in the Physical Sciences. Second edition. John Wiley and Sons, New York.

Jackson, J. E., 1980. Sphere, Spheroid and Projections for Surveyors. Granda Publishing, London.

Jaeger, J. C. and N. G. W. Cook, 1976. Fundamentals of Rock Mechanics. Chapman and Hall, London.

MacAyeal, D. R., 1985. Optimal Measurement of Ice Sheet Deformation From Surface Marker Arrays, Journal of Glaciology, Volume 31, Number 107.

Shabtaie, S. and C. R. Bentley, 1987. West Antarctic Ice Streams Draining into the Ross Ice Shelf: Configuration and Mass Balance, Journal of Geophysical Research, Volume 92, Number B2.

Thomas, R. H., D. R. MacAyeal, D. H. Eilers, and D. R. Gaylord, 1984. Glaciological Studies on the Ross Ice Shelf. Antarctic Research Series, Volume 42. American Geophysical Union.

Wager, A. C., C. S. M. Doake, J. G. Paren, and J. L. W. Walton, 1980. Survey Reduction for Glacier Movement Studies, Survey Review, Vol. 25.

APPENDIX 1 STATION COORDINATES

APPENDIX 2 STATIONS OCCUPIED ONCE WITH GEOCEIVERS BY NASA FIELD PARTIES (AS OF JAN 1986)

APPENDIX 3 DETAILS OF MULTI-LEG ROSETTE TECHNIQUE

APPENDIX 4 SCIENTIFIC PUBLICATIONS

APPENDIX 1: STATION COORDINATES

STATION	GEOGRAPHIC		POLAR STEROGRAPHIC		GRID		SOURCE
	d m s	d m s	(km)	(km)	d m s	d m s	
CRARY							
CAMP	83 37 15	166 44 30	162.484	-689.595	6 12 33	1 27 47	g2
	83 37 08	166 45 20	162.366	-689.845	6 12 41	1 27 43	g3
O	83 47 14	166 01 28	166.631	-669.539	6 01 44	1 30 02	g2
	83 47 07	166 02 43	166.440	-669.810	6 01 53	1 29 55	g3
A1	83 52 41	165 07 48	174.469	-657.088	5 55 01	1 34 16	s1
A2	83 57 29	164 16 24	181.861	-645.838	5 48 57	1 38 16	g3
B1	83 55 13	165 58 09	163.688	-655.015	5 53 54	1 28 26	s1
	83 55 16	166 00 02	163.307	-655.015	5 53 54	1 28 14	s2
B2	84 02 58	165 56 21	160.540	-640.990	5 46 20	1 26 45	s1
	84 03 02	165 57 31	160.292	-640.924	5 46 18	1 26 36	s2
C1	83 53 00	166 46 17	155.442	-661.244	5 57 16	1 23 59	s2
C2	83 57 32	167 41 16	143.054	-655.433	5 54 08	1 17 18	g3
C3	84 26 08	166 57 08	139.486	-601.891	5 25 15	1 15 22	g3
C4	84 57 52	165 38 44	138.596	-541.585	4 52 42	1 14 54	g2
	84 57 50	165 38 32	138.643	-541.637	4 52 44	1 14 56	g3
D1	83 47 37	167 12 13	152.660	-672.133	6 03 08	1 22 29	s1
	83 47 40	167 13 29	152.392	-672.099	6 03 07	1 22 20	s2
D2	83 47 44	168 22 02	138.936	-674.883	6 04 37	1 15 04	s1
E1	83 42 08	166 52 00	158.921	-681.128	6 07 59	1 25 52	s1
	83 42 25	166 52 29	158.706	-680.638	6 07 43	1 25 44	s2
E2	83 36 38	167 41 37	151.249	-693.317	6 14 34	1 21 43	s1
E1'	83 35 14	168 07 42	146.518	-696.986	6 16 32	1 19 09	e1
E2'	83 33 32	167 52 18	150.301	-699.406	6 17 50	1 21 12	e1
E2.3A	83 33 09	168 12 43	146.290	-700.982	6 18 42	1 19 02	g2
	83 33 05	168 13 14	146.211	-701.128	6 18 46	1 18 59	g3
E2.5	83 30 04	168 39 35	141.932	-707.712	6 22 19	1 16 40	e1
E3	83 22 44	169 34 34	133.057	-723.272	6 30 43	1 11 53	g2
	83 22 45	169 34 30	133.065	-723.238	6 30 42	1 11 53	g3
E4	83 09 20	171 36 38	110.924	-752.137	6 46 16	0 59 55	g2
	83 09 20	171 36 40	110.917	-752.138	6 46 16	0 59 55	g3
F1	83 39 43	166 01 13	170.048	-683.055	6 09 01	1 31 52	s1
	83 39 44	165 58 18	170.620	-682.881	6 08 56	1 32 11	s2
F2	83 31 59	166 02 37	173.229	-697.045	6 16 34	1 33 35	s1
	83 31 55	166 02 57	173.192	-697.182	6 16 38	1 33 34	s2
G1	83 41 38	165 06 18	180.024	-676.816	6 05 39	1 37 16	s1
G2	83 35 38	164 23 28	191.437	-685.239	6 10 12	1 43 25	g3
G3	83 25 42	162 43 09	216.822	-696.957	6 16 30	1 57 08	g2
	83 25 33	162 43 45	216.783	-697.260	6 16 40	1 57 06	g3
G4	83 16 40	161 26 55	237.555	-707.867	6 22 23	2 08 19	g2
	83 16 32	161 27 17	237.558	-708.127	6 22 31	2 08 20	g3
H1	83 47 02	164 48 42	180.862	-666.220	5 59 56	1 37 43	s1
	83 46 58	164 48 44	180.888	-666.342	6 00 00	1 37 44	s2
H2	83 46 09	163 40 13	194.558	-664.058	5 58 46	1 45 07	g3
J1	83 35 26	171 35 33	104.081	-704.199	6 20 26	0 56 14	g2
	83 35 19	171 37 00	103.816	-704.457	6 20 34	0 56 05	g3
J2	83 19 04	173 04 26	89.503	-736.795	6 38 00	0 48 21	g2
	83 18 56	173 05 32	89.297	-737.069	6 38 09	0 48 14	g3
J3	83 07 22	174 55 29	67.580	-760.927	6 51 01	0 36 30	g2
	83 07 12	174 56 21	67.415	-761.252	6 51 11	0 36 25	g3
K1	83 10 24	168 09 09	155.683	-742.140	6 40 52	1 24 06	g2

	83 10 18	168 09 44	155.595	-742.348	6 40 59	1 24 03	g3
K2	82 56 35	169 57 59	136.582	-771.946	6 56 56	1 13 46	g2
	82 56 29	169 58 35	136.479	-772.152	6 57 03	1 13 43	g3
K3	82 49 26	171 09 53	122.447	-787.748	7 05 28	1 06 08	g2
	82 49 21	171 10 36	122.306	-787.926	7 05 33	1 06 03	g3
L1	83 06 12	172 25 21	101.022	-759.397	6 50 11	0 54 34	g2
	83 06 11	172 25 23	101.018	-759.429	6 50 12	0 54 34	g3
LP1	83 00 04	172 59 57	94.761	-771.674	6 56 48	0 51 11	g2
	83 00 05	172 59 53	94.772	-771.641	6 56 47	0 51 11	g3
DOWNSTREAM B							
DNB	84 10 28	154 18 43	280.431	-582.938	5 14 59	2 31 31	g2
	84 10 28	154 21 24	279.950	-583.169	5 15 06	2 31 16	g3
A11	84 18 16	154 30 54	272.116	-570.887	5 08 29	2 27 02	e2
A19	84 24 27	154 42 21	265.316	-561.428	5 03 23	2 23 21	g2
	84 24 26	154 45 03	264.888	-561.664	5 03 30	2 23 08	g3
B10	84 02 42	154 07 06	288.659	-594.954	5 21 28	2 35 58	e2
B18	83 57 00	153 33 32	299.160	-601.571	5 25 02	2 41 38	g2
	83 56 58	153 35 42	298.809	-601.815	5 25 10	2 41 27	g3
B25	83 52 02	153 10 38	307.331	-607.811	5 28 23	2 46 02	g2
	83 52 02	153 10 42	307.305	-607.790	5 28 23	2 46 02	g3
C10	84 12 53	153 06 35	290.548	-572.943	5 09 35	2 36 60	e2
E10	84 10 44	155 37 12	266.821	-588.749	5 18 07	2 24 10	e2
E19	84 09 03	156 51 07	255.328	-597.219	5 22 42	2 17 58	g2
	84 09 01	156 53 31	254.935	-597.454	5 22 49	2 17 45	g3
G1	84 03 58	152 08 59	307.847	-582.632	5 14 48	2 46 19	g2
	84 03 58	152 11 46	307.358	-582.860	5 14 56	2 46 04	g3
G2	84 00 28	150 32 03	327.325	-579.350	5 13 02	2 56 51	g2
	84 00 31	150 34 49	326.813	-579.533	5 13 08	2 56 35	g3
H2	83 53 49	150 25 25	334.528	-589.442	5 18 28	3 00 44	g2
	83 53 50	150 25 29	334.502	-589.422	5 18 28	3 00 44	g3
M0	84 17 46	158 10 58	235.383	-587.986	5 17 43	2 07 11	g2
	84 17 42	158 13 27	235.004	-588.271	5 17 52	2 06 59	g3
M1	84 22 05	156 53 27	245.440	-575.170	5 10 48	2 12 38	e3
M2	84 25 40	158 07 53	230.456	-574.185	5 10 16	2 04 32	g3
M3	84 21 12	159 26 11	220.227	-587.036	5 17 13	1 59 00	g3
M4	84 13 28	159 29 32	224.677	-600.678	5 24 34	2 01 24	s2
M5	84 10 01	158 15 49	239.874	-601.663	5 25 06	2 09 37	s2
M6	84 13 17	157 05 06	249.841	-591.024	5 19 21	2 14 60	s2
N1	83 50 30	161 56 00	212.095	-650.186	5 51 17	1 54 35	g3
N2	83 36 11	160 22 29	238.619	-669.187	6 01 31	2 08 55	g3
N3	83 46 55	157 07 35	268.417	-636.248	5 43 45	2 25 01	g3
N4	84 03 44	159 01 17	236.066	-615.660	5 32 39	2 07 33	g3
DOWNSTREAM C							
DNC	82 49 18	152 26 55	368.858	-707.021	6 21 51	3 19 13	g2
A1	82 59 48	152 28 50	359.458	-689.941	6 12 39	3 14 09	g2
A2	83 10 43	152 30 45	349.723	-672.169	6 03 05	3 08 54	g2
A3	83 18 42	152 32 05	342.620	-659.161	5 56 04	3 05 05	g2
B1	82 38 48	152 25 46	378.117	-724.178	6 31 06	3 24 12	g2
B2	82 30 50	152 24 33	385.225	-737.155	6 38 05	3 28 02	g2
B3	82 18 07	152 23 07	396.480	-757.922	6 49 16	3 34 06	g2
C1	82 49 11	151 21 23	382.372	-700.051	6 18 06	3 26 31	g2
C2	82 49 02	150 15 28	395.862	-692.833	6 14 12	3 33 48	s1
C3	82 42 46	149 06 00	415.755	-694.676	6 15 10	3 44 32	g2

D19	82	48	55	155	17	34	333.619	-725.099	6	31	37	3 00 11	g2
H5	82	35	24	153	15	02	370.542	-735.160	6	37	01	3 20 07	g2
WISCONSIN STATIONS ON ROSS ICE SHELF													
C2	83	57	32	167	41	16	143.054	-655.433	5	54	08	1 17 18	g3
W3	84	55	53	155	44	05	231.253	-512.998	4	37	15	2 04 59	
W4	84	49	29	161	02	39	186.643	-543.411	4	53	41	1 40 52	g3
W4525	84	56	05	154	37	46	240.947	-508.107	4	34	36	2 10 13	g3
W5	84	35	31	166	37	35	138.884	-584.169	5	15	41	1 15 03	g3
W6	84	25	14	169	21	55	114.329	-608.869	5	29	01	1 01 47	g3
W9	84	19	10	159	46	37	218.037	-591.872	5	19	49	1 57 49	g3

SOURCES:

g2: GEOCEIVER FIX FROM 1984-1985 FIELD SEASON
g3: GEOCEIVER FIX FROM 1985-1986 FIELD SEASON
s1: SAT NAV FIX FROM 1983-1984 FIELD SEASON
s2: SAT NAV FIX FROM 1984-1985 FIELD SEASON
e1: EXTRAPOLATION USING GEOC. POSITION OF E2.3A AND SKIDOO ODOMETER
e2: EXTRAPOLATION USING GEOC. POSITION OF DNB AND SKIDOO ODOMETER
e3: EXTRAPOLATION USING GEOC. POSITION OF MO

APPENDIX 2: STATIONS OCCUPIED ONCE WITH GEOCEIVERS BY NASA FIELD PARTIES (AS OF JANUARY 1986)

SITE	LATITUDE	LONGITUDE	EL (m)	PA	TIME	DATE
CRARY						
C3	84 26 07.625	166 57 08.402	56	47	15 35	24 11 85
H2	83 46 09.281	163 40 14.034	50	25	20 00	18 12 85
A2	83 57 28.588	164 16 24.332	48	58	3 35	1 12 85
G2	83 35 37.797	164 23 28.932	39	12	13 8	27 11 85
F1	83 39 27.587	166 02 54.77	40	24	7 45	22 11 85
DOWNSTREAM B						
M2	84 25 40.249	158 07 52.608	70	34	06 00	10 12 85
M3	84 21 12.548	159 26 10.863	56	8	8 29	10 12 85
N1	83 50 29.663	161 56 00.344	49	27	11 40	4 12 85
N2	83 36 11.064	160 22 29.464	52	28	00 45	4 12 85
N3	83 46 55.426	157 07 35.203	55	50	20 00	2 12 85
N4	84 03 44.258	159 01 16.731	70	6	05 59	3 12 85
DOWNSTREAM C						
O	82 49 17.859	152 26 55.258	99	25	21 51	25 12 84
A1	82 59 48.191	152 28 49.899	91	24	1 38	29 12 84
A2	83 10 42.763	152 30 44.793	86	6	7 40	29 12 84
A3	83 18 42.206	152 32 04.592	74	17	19 25	29 12 84
B2	82 30 49.841	152 24 33.203	63	16	23 44	31 12 84
B3	82 18 07.056	152 23 07.012	107	1	3 3	31 12 84
C1	82 49 10.783	151 21 22.814	116	16	20 52	30 12 84
C3	82 42 45.673	149 06 00.324	124	8	7 36	3 1 85
F1	82 48 54.844	155 17 33.593	30	42	20 13	3 1 85
WISCONSIN STATIONS ON ROSS ICE SHELF						
W6	84 25 13.521	169 21 54.822	50	23	18 28	2 12 85
W5	84 35 30.675	166 37 34.879	59	5	05 24	2 12 85
W4525	84 56 04.558	154 37 46.514	94	20	00 56	3 12 85
C2	83 57 31.509	167 41 15.866	45	7	02 05	2 12 85
W9	84 19 10.379	159 46 36.782	62	22	23 16	3 12 85
W4	84 49 28.752	161 02 39.241	72	56	10 4	5 12 85

APPENDIX 3: DETAILS OF MULTI-LEG ROSETTE TECHNIQUE

Four multi-leg rosettes were planted between 1st December and 6th December, 1985 by two independent two-man survey teams. At each site, four central stakes (labeled 01 to 04) were planted into the snow using post levels to maintain verticality. These four central stakes were positioned to form the corners of a square with 150-m sides. Ten outlying stakes were positioned in an array surrounding the central square. Their distance from the central square was approximately 1500 m, and they were separated from each other by an angle of 36 degrees about 01.

Distances were measured between each of the four central stakes and the ten outlying stakes using a Geodimeter 112 EDM with a nominal accuracy of 0.01 m over 1500 m; the times of each measurement were recorded to the nearest minute. Rounds of angles between a reference outlying stake, 'A' and the other 9 outlying stakes were measured using a Wild T-2 theodolite to a nominal accuracy of 3 seconds of arc, mounted on a tripod optically plumbed over the center of each of the four central stakes. The commencement time of each round was recorded. The true azimuth of the 'A' stake from each of the four central stakes was measured using observations onto the sun. The Magnavox MX1502 geoceiver provided both the time and the longitude used for the calculation of azimuth. The estimated error is 15 seconds of arc. This is greater than the error in observing angles between the outlying stakes, but the azimuth is only used to determine the relative vorticity (rigid body rotation). The geoceiver was also used to determine the geodetic position of one of the central stakes to an estimated error of 20 meters, (see Section 1).

Resurvey of three of the four multi-leg rosettes was accomplished using the same measurement techniques by one two-man survey party between 16 December and 19 December, 1985. After the resurvey, three outlying stakes and one central stake were extended so that the station could be resurveyed in the future as a 3-leg rosette.

Data Organization

The observed relative position of the Nth outlying stake with respect to each of the four central stakes is described in polar coordinates ($R_n, \Theta_n, t_{R_n}, t_{\Theta_n}$) where R_n denotes the radial distance, Θ_n denotes the true azimuth (determined by adding the azimuth of the 'A' stake to the angular separation between the 'A' stake and the Nth stake), and t_{R_n} and t_{Θ_n} denote the times at which R_n and Θ_n are observed.

The four sets of ten relative positions were combined to comprise one set of 40 relative positions. The effect of lumping the data together in this manner is to average out any strain rate gradients within the 150-m box formed by the four central stakes. This averaging is not considered detrimental because our primary objective is to determine the average strain rate within the whole rosette and not the strain rate gradient.

Another modification made to the data was that the initial observations of the 'A' stake's azimuth were substituted for the final observations of the azimuth made during the resurvey. This was done to avoid introducing the azimuth uncertainty into the determination of stake displacements. Effectively, the azimuth data is used to determine the average positions of the stakes with respect to each other, but not to determine their relative displacements. Comparisons were made between strain rate reductions in which this substitution was and was not done, and no significant differences (they were less than 0.01 times the standard deviation of the strain rate components) were noticed. The relative vorticity determined as a result of this substitution must be corrected by adding the relative vorticity associated with the 'rigid rotation' determined by the rate of change of the true azimuth. We describe the uncertainty associated with the determination of the relative vorticity separately, below.

Once two sets of 40 stake positions representing the initial and final survey are established, average positions $\bar{R}_n$, $\bar{\Theta}_n$ and relative velocities $\dot{R}_n$, $\dot{\Theta}_n$ are computed:

$$\bar{R}_n = \tfrac{1}{2}(R_n^i + R_n^f) \tag{1}$$

$$\bar{\Theta}_n = \tfrac{1}{2}(\Theta_n^i + \Theta_n^f) \tag{2}$$

$$\dot{R}_n = \frac{R_n^f - R_n^i}{t_{R_n}^f - t_{R_n}^i} \tag{3}$$

$$\dot{\Theta}_n = \frac{\Theta_n^f - \Theta_n^i}{t_{\Theta_n}^f - t_{\Theta_n}^i} \tag{4}$$

where superscripts i and f denote values determined during the initial and final surveys, respectively.

These data are next converted to average positions $\bar{x}_n$, $\bar{y}_n$ and relative velocities $\dot{x}_n$, $\dot{y}_n$ in a coordinate system having an X-axis aligned with true North and a Y-axis aligned with true West,

$$\bar{x}_n = \bar{R}_n \cos \bar{\Theta}_n \tag{5}$$

$$\bar{y}_n = - \bar{R}_n \sin \bar{\Theta}_n \tag{6}$$

$$\dot{x}_n = \dot{\bar{R}}_n \cos \bar{\Theta}_n - \bar{R}_n \sin \bar{\Theta}_n \dot{\Theta}_n \quad (7)$$

$$\dot{y}_n = - \dot{\bar{R}}_n \sin \bar{\Theta}_n - \bar{R}_n \cos \bar{\Theta}_n \dot{\Theta}_n \quad (8)$$

Determination of Strain Rates

The determination of strain rates from a 40-leg, over-determined stake velocity data set requires a least-squares procedure known as singular value decomposition. Here we outline the details of this calculation.

The strain rates are determined from the gradients in u and v where u and v are components of the velocity in the x and y directions, respectively (following Jaeger and Cook, 1976). The first step is to determine these velocity gradients by solving for S, the least-squares estimate of the velocity gradient column vector, in the following equation. (Note that here we write the equations in terms of a 40-leg rosette; the equations are easily modified to address an N-leg rosette where N is arbitrary.)

$$\underline{\underline{A}} \times \underline{S} = \underline{d} - \underline{z} \quad (9)$$

where,

$$\underline{\underline{A}} = \begin{bmatrix} \bar{x}_1 & \bar{y}_1 & O & O \\ \vdots & \vdots & \vdots & \vdots \\ \bar{x}_{40} & \bar{y}_{40} & O & O \\ O & O & \bar{x}_1 & \bar{y}_1 \\ \vdots & \vdots & \vdots & \vdots \\ O & O & \bar{x}_{40} & \bar{y}_{40} \end{bmatrix} \qquad \underline{S} = \begin{bmatrix} \frac{\partial u}{\partial x} \\ \frac{\partial u}{\partial y} \\ \frac{\partial v}{\partial x} \\ \frac{\partial v}{\partial y} \end{bmatrix}$$

$$\underline{d} = \begin{bmatrix} \dot{x}_1 \\ \vdots \\ \dot{x}_{40} \\ \dot{y}_1 \\ \vdots \\ \dot{y}_{40} \end{bmatrix} \qquad \underline{z} = \begin{bmatrix} z_1 \\ \vdots \\ z_{40} \end{bmatrix}$$

and z represents the measurement error in the observed values of d. We assume that the covariance of $\underline{z}$ is given by:

$$i = 1,40 \qquad \mathrm{cov}(z_i, z_j) = \left\{ \frac{\sigma_R^2 \cos^2 \bar{\theta}_i}{(t_{R_i}^f - t_{R_i}^l)^2} + \frac{\sigma_\theta^2 \bar{R}_i^2 \sin^2 \bar{\theta}_i}{(t_{\theta_i}^f - t_{\theta_i}^l)^2} \right\} \delta_{ij} \qquad (10)$$

$$i = 41,80 \quad \text{cov}(z_i,z_j) = \left\{ \frac{\sigma_R^2 \sin^2 \bar{\Theta}_i}{(t^f_{R_i} - t^i_{R_i})^2} + \frac{\sigma_\Theta^2 \bar{R}_i^2 \cos^2 \Theta_i}{(t^f_{\Theta_i} - t^i_{\Theta_i})^2} \right\} \hat{o}_{ij}$$

where $\hat{o}_{ij}$ is the Kroneker delta, σ_R is the standard deviation estimate of the measurments of R_n in meters, and σ_Θ is the standard deviation estimate of the measurement of Θ_n in radians. This assumes covariance is consistent with the assumption that each of the 40 measurements of the stake velocities are statistically independent. However, the measurements are not completely independent because certain types of error associated with disturbing outlying stakes can affect four of the data points, one each associated with the observation from each central stake. We assume that these statistical dependencies produce only small off-diagonal terms in the covariance matrix of z compared to the diagonal terms. As stated previously, we assume that σ_R =0.01 m and σ_Θ =3 sec in radians.

To correct for some components of z being larger than others by virtue of the inequality of σ_R and $\bar{R}_n\sigma_\Theta$, we weight the data matrix $\underline{d}$ and the position matrix $\underline{\underline{A}}$,

$$d_i^w = d_i \left[\frac{\sigma^2}{\text{cov}(z_i, z_i)} \right]^{1/2} \tag{11}$$

$$A_{ij}^w = A_{ij} \left[\frac{\sigma^2}{\text{cov}(z_i, z_i)} \right]^{1/2} \tag{12}$$

and,

$$z_i^w = z_i \left[\frac{\sigma^2}{\text{cov}\,(z_i, z_i)} \right]^{1/2} \tag{13}$$

where the superscript w's denote weighted elements, and

$$\sigma^2 = \frac{1}{80} \sum_{i=1}^{80} \text{cov}\,(z_i, z_i) \tag{14}$$

Equation (9) now becomes,

$$\underline{\underline{A}}^w \times \underline{S} = \underline{d}^w + \underline{z}^w \tag{15}$$

where the covariance matrix of $\underline{z}^w$ is now σ^2 on the diagonal.

To invert $\underline{\underline{A}}^w$ for determining $\underline{S}_{ij}$, the four eigenvalues λ_k and the eigenvectors $\underline{r}_k$ of $[\underline{\underline{A}}^w]^T[\underline{\underline{A}}^w]$ are computed:

$$\lambda_1 = \frac{\alpha_1 + \gamma_1}{2} + \left\{ \frac{(\alpha_1 + \gamma)^2}{4} - (\alpha_1\gamma_1 - \beta_1^2) \right\}^{1/2} \tag{16}$$

$$\lambda_2 = \frac{\alpha_1 + \gamma_1}{2} - \left\{ \frac{\alpha_1 + \gamma_1}{4} - (\alpha_1\gamma_1 - \beta_1^2) \right\}^{1/2} \tag{17}$$

$$\lambda_3 = \frac{\alpha_2 + \gamma}{2} - \left\{ \frac{(\alpha_2 + \gamma_2)^2}{4} - (\alpha_2\gamma_2 - \beta_2^2) \right\}^{1/2} \tag{18}$$

$$\lambda_4 = \frac{\alpha_2 + \gamma_2}{2} - \left\{ \frac{(\alpha_2 + \gamma_2)^2}{4} - (\alpha_2\gamma_2 - \beta_2^2) \right\}^{1/2} \tag{19}$$

and,

$$\underline{r}_1^T = \left(\frac{-\beta_1}{\alpha_1 - \lambda_1} \left(1 + \frac{\beta_1^2}{(\alpha_1 - \lambda_1)^2} \right)^{-1/2}, \left(1 + \frac{\beta_1^2}{(\alpha_1 - \lambda_1)^2} \right)^{-1/2}, 0, 0 \right) \tag{20}$$

$$\underline{r}_2^T = \left(\frac{\alpha_1 - \lambda_1}{\beta_1} \left(1 + \frac{(\alpha_1 - \lambda_1)^2}{\beta_1} \right)^{-1/2}, \left(1 + \frac{(\alpha_1 - \lambda_1)^2}{\beta_1} \right)^{-1/2}, 0, 0 \right) \tag{21}$$

$$\underline{r}_3^T = \left(0, 0, -\frac{\beta_2}{\alpha_2 - \lambda_3} \left(1 + \frac{\beta_2^2}{(\alpha_2 - \lambda_3)^2} \right)^{-1/2}, \left(1 + \frac{\beta_2^2}{(\alpha^2 - \lambda_3)^2} \right)^{-1/2} \right) \tag{22}$$

$$\underline{r}_4^T = \left(0, 0, \frac{\alpha_2 - \lambda_3}{\beta_2} \left(1 + \frac{(\alpha_2 - \lambda_3)^2}{\beta_2^2} \right)^{-1/2}, \left(1 + \frac{\beta_2^2}{(\alpha_2 - \lambda_3)^2} \right)^{-1/2} \right) \tag{23}$$

and where,

$$[\underline{\underline{A}}^w]^T[\underline{\underline{A}}^w] = \begin{bmatrix} \alpha_1 & \beta_1 & 0 & 0 \\ \beta_1 & \gamma_1 & 0 & 0 \\ 0 & 0 & \alpha_2 & \beta_2 \\ 0 & 0 & \beta_2 & \gamma_2 \end{bmatrix} \tag{24}$$

with

$$\alpha_1 = \sum_{i=1}^{40} \left[\frac{\sigma^2}{\text{cov}\ (z_i,\ z_i)} \right] \bar{x}_i^2 \qquad (25)$$

$$\beta_1 = \sum_{i=1}^{40} \left[\frac{\sigma^2}{\text{cov}\ (z_i,\ z_i)} \right] \bar{x}_i\ \bar{y}_i \qquad (26)$$

$$\gamma_1 = \sum_{i=1}^{40} \left[\frac{\sigma^2}{\text{cov}\ (z_i,\ z_i)} \right] \bar{y}_i^2 \qquad (27)$$

$$\alpha_2 = \sum_{i=1}^{40} \left[\frac{\sigma^2}{\text{cov}\ (z_{i+40},\ z_{i+40})} \right] \bar{x}_i^2 \qquad (28)$$

$$\beta_2 = \sum_{i=1}^{40} \left[\frac{\sigma^2}{\text{cov}\ (z_{i+40},\ z_{i+40})} \right] \bar{x}_i\ \bar{y}_i \qquad (29)$$

and,

$$\gamma_2 = \sum_{i=1}^{40} \left[\frac{\sigma^2}{\text{cov}\ (z_{i+40},\ z_{i+40})} \right] \bar{y}_i^2 \qquad (30)$$

The least-squares estimate of $\underline{S}$ is found by constructing the inverse of A,

$$[\underline{A}^{w}]^{-1} = \underline{\underline{R}} \cdot \underline{\underline{\Gamma}}^{-1} \cdot \underline{\underline{Q}}^{T} \tag{31}$$

where R, Γ and Q are matrices defined in MacAyeal (1985). In component notation,

$$S_i = \sum_{k=1}^{4} r_i^k \frac{1}{\lambda_k} \left\{ \sum_{\ell=1}^{40} \left(\bar{x}_\ell \, r_1^k + \bar{y}_\ell \, r_2^k \right) \frac{\sigma^2}{\mathrm{cov}\,(z_\ell, z_\ell)} d_\ell \right. \tag{32}$$

$$\left. + \sum_{\ell=41}^{80} \left(\bar{x}_{\ell-40} \, r_3^k + \bar{y}_{\ell-40} \, r_4^k \right) \frac{\sigma^2}{\mathrm{cov}\,(z_\ell, z_\ell)} d_\ell \right\}$$

where the superscript k refers to the eigenvector number.

The principal axes e1 and e2 of the horizontal strain rate tensor are determined from $\underline{S}$ by using the relations (Jaeger and Cook, 1976)

$$\Theta = \tfrac{1}{2} \tan^{-1} \left(\frac{S_2 + S_3}{S_1 + S_4} \right) \tag{33}$$

$$\dot{e}_1 = S_1 \cos^2 \theta + \tfrac{1}{2} (S_2 + S_3) \sin 2\theta + S_4 \sin^2 \theta \qquad (34)$$

and

$$\dot{e}_2 = S_1 \sin^2 \theta - \tfrac{1}{2} (S_2 + S_3) \sin 2\theta + S_4 \cos^2 \theta \qquad (35)$$

where θ is the counterclockwise angle (in radians) between the x-axis, or north, and the e1-axis.

Computation of Error

Perhaps the most critical element of our analysis is the computation of expected uncertainty for the derived values of θ, $\dot{e}_1$, $\dot{e}_2$, and $\dot{e}_{zz} = -\dot{e}_1 - \dot{e}_2$. This is critical for two reasons. Firstly, the short time period over which the 40-leg rosette was allowed to deform means that the observed stake displacements may be close to the limits of detectability, and secondly, the value of one of the strain rate principal components may be several orders of magnitude less than the maximum component and its value may be statistically insignificant.

The expected uncertainty, or estimated standard deviation of the components of $\underline{S}$, are determined formally through the singular value decomposition procedure (MacAyeal, 1985).

$$\sigma_{S_i} = \left[\mathrm{cov}(S_i - S_i^*, S_i - S_i^*) \right]^{1/2} \qquad (36)$$

where S^* is composed of the 'true' value of the velocity gradients, and $\underline{S}$ is, as stated before, the least-squares estimate of S^*. Observe that the components of σ depend only on the covariance of z^w, the eigenvectors and the eigenvalues of $[A^w]^T[A^w]$; the latter two of which depend only on stake positioning.
In component notation,

$$\sigma_{S_i} = \left\{ \sum_{k=1}^{4} \sum_{i=1}^{4} \frac{r_i^i \, r_k^i}{\lambda_k} \cdot \sigma^2 \right\}^{1/2} \qquad (37)$$

where σ^2 is given by Equation (14), and subscripts i refer to eigenvector number.

The uncertainty of Θ, $\dot{e}_1$, $\dot{e}_2$ are computed from the σ_{S_i}'s using the relationship for functions of random variables (Boas, 1983).

$$\sigma_\Theta = \tfrac{1}{2} \left(1 + \frac{S_2 - S_3}{S_1 + S_4} \right) \left\{ \left(\frac{S_2 + S_3}{(S_1 - S_4)^2} \right)^2 (\sigma_{S_1}^2 + \sigma_{S_4}^2) + \left(\frac{1}{S_1 - S_4} \right)^2 (\sigma_{S_2}^2 + \sigma_{S_3}^2) \right\}^{1/2} \qquad (38)$$

$$\sigma_{\dot{e}_1} = \left| \cos^4 \Theta \, \sigma_{S_1}^2 + \tfrac{1}{4} \sin^2 2\Theta (\sigma_{S_2}^2 + \sigma_{S_3}^2) + \sin^4 \Theta \, \sigma_{S_4}^2 + \left((S_4 - S_1) \sin 2\Theta + (S_2 + S_3 \cos 2\Theta)^2 \right) \sigma^2 \right|^{1/2} \qquad (39)$$

and,

$$\sigma_{\dot{e}_2} = \{\sin^4\Theta\,\sigma^2_{S_1} + \tfrac{1}{4}\sin^2 2\Theta(\sigma^2_{S_2} + \sigma^2_{S_3}) + \cos^4\Theta\,\sigma^2_{S_4} + \left((S_1 - S_4)\sin 2\Theta - (S_2 + S_3)\cos 2\Theta\right)^2 \sigma^2_{(\cdot)}\}^{1/2} \quad (40)$$

Data reduction programs

The above technique for reducing 40-leg rosette data can be used to reduce any rosette design (including the standard 3-leg rosette), or other strain figures which yield data in the form $\overline{x_i}$, $\overline{y_i}$, x_i, and y_i. A reliable calculator program which will reduce rosettes having up to 100 legs (a limit imposed by the size of calculator memory) has been developed and tested. This program was tested by two means. First, the results of reducing several 3-leg rosettes were compared with results using other methods, and second, multi-leg rosette data were synthesized using a known strain rate, and then reduced by the program to test whether the known strain rate is reproduced. This program, available on request, requires the following equipment: Hewlett-Packard 41-CX hand calculator having "Date" and "Time" functions and at least 3 modules for memory extension, an HP magnetic card reader to input the program, and an HP thermal printer to verify correct data input. The use of a hand calculator was chosen to allow data reduction in the field and this battery powered equipment operated well within the tented shelters used during the field program.

Results

Here, we present information comparing the SVD method with other methods of data reduction. First, the SVD method is compared to the method used in Section 2 of this report for calculating

strain rates from 3-leg rosette data to check the reliability of both these methods. Second, subsets of the 40-leg rosette data are used, which illustrate that the derived strain rate converges as the number of legs is increased.

Table 18 presents strain rates derived by both methods from 3-leg strain rosettes surrounding the Crary Ice Rise. To illustrate the effect of weighting, Table 18 also includes results obtained when the data is not weighted in the SVD method. It is seen that data weighting may be considered unnecessary in the analysis of 3-leg rosette data because errors in the distance and angle measurements are insignificant compared to actual changes in those quantities over the survey period. For all 14 stations, the principal horizontal strain rate components derived by the two methods differed by less than 10 percent and fall within the computed uncertainty limits obtained by both methods. This comparison serves as a useful check on both our data-analysis techniques.

To illustrate convergence of the SVD technique in producing an accurate estimate of the horizontal strain rates from the 40-leg rosette N3, twelve independent 3-leg rosettes and four independent 10-leg rosettes from the 40-leg rosette data are synthesized by considering subsets of the stake array. The results are given in Table 18. There is considerable scatter in the results of the twelve 3-leg rosette as expected from the short time period before which the 3-leg rosettes were resurveyed, but the strain rate falls within the sample standard deviation of the strain rate derived from the analysis of the 40-leg data. The sample standard deviation of the twelve 3-leg rosettes results is larger than the confidence limits computed from 40-leg rosette data. This could have resulted from three factors: 1) our estimates of measurement error on R and Θ are too low, 2) the sample of twelve 3-leg rosettes is too small to produce an accurate sample standard deviation, and 3) there is strain rate variation within the confines of our stake array that is averaged out by the 40-leg analysis. All these possible

explanations have some validity. However, the possible underestimate of the measurement accuracy seriously affects the scientific conclusions of our study; certainly any underestimate is not a factor of 10, which is needed if that alone causes the discrepancy.

As another illustration of the multi-leg rosette analysis, four 10-leg rosette sub-sets were analyzed, each of the 4 central stakes being the center of a separate stake array. There is much less scatter in these results (Table 18) when compared to the twelve 3-leg rosettes. The sample standard deviation is also consistent with the confidence limits of the 40-leg rosette showing there is a convergence in both the derived strain rate and the confidence limits as the number of stakes is increased.

INSTRUMENT CORRECTIONS

Benchmark comparisons were made periodically between all EDM's used in the 1985-1986 field season. These comparisons revealed that 1 EDM used in the initial and final surveys of 40-leg stations N1 and N4 requires a $-5.5 \times 10^{-5} + 0.1 \times 10^{-5}$ parts-per-part correction to the initial measured distance.

MULTI-LEG ROSETTE UTILITY

Multi-leg rosettes can serve a useful purpose under circumstances when more practical 3-leg rosettes will not provide sufficient accuracy over the time interval between survey and resurvey. Consideration must be taken of the large commitment in time required to deploy these rosettes. Experienced surveyors, in good weather, needed 1.5 days to deploy a 40-leg rosette and 1 day to resurvey it. The method also requires instrument dependability.

APPENDIX 4: SCIENTIFIC PUBLICATIONS

1) Bindschadler, R.A., B. Koci, S. Shabtaie, and E.P. Roberts, in press. Evolution of Crary Ice Rise, Antarctica, Annals of Glaciology, **12**.

2) Bindschadler, R.A., P.L. Vornberger, S.N. Stephenson, E.P. Roberts, S. Shabtaie, and D.R. MacAyeal, in press. Ice-Shelf Flow at the Boundary of Crary Ice Rise, Annals of Glaciology, **11**.

3) Bindschadler, R.A., D.R. MacAyeal, and S.N. Stephenson, 1987. Ice Stream-Ice Shelf Interaction in West Antarctica. In The Dynamics of the West Antarctic Ice Sheet (C.J. Van der Veen and J. Oerlemans, eds.), D. Reidel Pub. Co., p. 161-180.

4) Bindschadler, R.A., S.N. Stephenson, D.R. MacAyeal, and S. Shabtaie, 1987. Ice Dynamics at the Mouth of Ice Stream B, Antarctica, J. Geophys. Res., **92**, No. B9, p. 8885-8894.

5) Lindstrom, D.R., submitted. West Antarctic Ice Sheet Formation, Annals of Glaciology, **11**.

6) Lindstrom, D.R. and D.R. MacAyeal, 1987. Environmental Constraints on West Antarctic Ice Sheet Formation, J. Glaciology, **33**, No. 115, p. 1-11.

7) MacAyeal, D.R., 1987. Ice-Shelf Backpressure: Form Drag vs. Dynamic Drag, In The Dynamics of the West Antarctic Ice Sheet (C.J. Van der Veen and J. Oerlemans, eds.), D. Reidel Pub. Co., p.141-160.

8) MacAyeal, D.R., R.A. Bindschadler, K.C. Jezek, and S.

Shabtaie, in press. Can Relict Crevasse Plumes on Antarctic Ice Shelves Reveal a History of Ice-Stream Fluctuation?, Annals of Glaciology, **11.**

9) MacAyeal, D.R., R.A. Bindschadler, S. Shabtaie, S.N. Stephenson, and C.R. Bentley, 1987. Force, Mass, and Energy Budgets of the Crary Ice Rise Complex, J. Glaciology, **33,** No. 114, p. 218-230.

10) Shabtaie, S., C.R. Bentley, R.A. Bindschadler, and D.R. MacAyeal, in press. Mass Balance Studies of Ice Streams A, B, and C and Possible Surging Behavior of Ice Stream B, Annals of Glaciology, **11.**

11) Stephenson, S.N. and R.A. Bindschadler, 1988. Observed Velocity Fluctuations on a Major Antarctic Ice Stream, Nature **334.**

12) Thomas, R.H., S.N. Stephenson, R.A. Bindschadler, S.Shabtaie, and C.R. Bentley, in press. Thinning and Grounding Line Retreat on the Ross Ice Shelf. Annals of Glaciology, **11.**

NASA

Report Documentation Page

1. Report No	2. Government Accession No.	3. Recipient's Catalog No
NASA TM-100708		

4. Title and Subtitle

Data Report for the Siple Coast Project

5. Report Date

October 1988

6. Performing Organization Code

671.0

7. Author(s)

R. A. Bindschadler, S. N. Stephenson, E. P. Roberts, D. R. MacAyeal, and D. R. Lindstrom

8. Performing Organization Report No.

88B0214

10. Work Unit No.

9. Performing Organization Name and Address

Goddard Space Flight Center
Greenbelt, Maryland 20771

11. Contract or Grant No.

13. Type of Report and Period Covered

Technical Memorandum

12. Sponsoring Agency Name and Address

National Aeronautics and Space Administration
Washington, D.C. 20546-0001

14. Sponsoring Agency Code

15. Supplementary Notes

S. N. Stephenson - Science Applications Research, Lanham, Maryland, 20706;
E. P. Roberts - Department of Geology, University of Maryland, College Park, Maryland, 20742;
D. R. MacAyeal and D. R. Lindstrom - Department of Geophysical Sciences, University of Chicago, Chicago, Illinois, 60637.

16. Abstract

This report presents data collected during three field seasons of glaciological studies in Antarctica and describes the methods employed. The region investigated covers the mouths of Ice Streams B and C (the Siple Coast) and Crary Ice Rise on the Ross Ice Shelf. Measurements included in the report are: surface velocity and deformation from repeated satellite geoceiver positions; surface topography from optical levelling; radar sounding of ice thickness; accumulation rates; near-surface densities and temperature profiles, and mapping from aerial photography.

17. Key Words (Suggested by Author(s))	18. Distribution Statement
Ice Sheet Glaciology Ice Dynamics	Unclassified - Unlimited Subject Category 43

19. Security Classif. (of this report)	20. Security Classif. (of this page)	21. No. of pages	22. Price
Unclassified	Unclassified		

National Aeronautics and
Space Administration

Washington, D.C.
20546

Official Business
Penalty for Private Use, $300

Postage and Fees Paid
National Aeronautics and
Space Administration
NASA-451

NASA

POSTMASTER: If Undeliverable (Section 158 Postal Manual) Do Not Return